frontiers | Frontiers in Earth Science

TYPE Original Research
PUBLISHED 06 February 2023
DOI 10.3389/feart.2023.1110568

OPEN ACCESS

EDITED BY
Changqian Ma,
China University of Geosciences Wuhan, China

REVIEWED BY
Fuhao Xiong,
Chengdu University of Technology, China
Anh Nong,
Ho Chi Minh City University of Science, Vietnam
Juliane Hennig-Breitfeld,
Chemostrat Ltd., United Kingdom

*CORRESPONDENCE
J. Gregory Shellnutt,
jgshelln@ntnu.edu.tw

SPECIALTY SECTION
This article was submitted to Petrology, a section of the journal Frontiers in Earth Science

RECEIVED 29 November 2022
ACCEPTED 19 January 2023
PUBLISHED 06 February 2023

CITATION
Shellnutt JG, Ma GS-K, Chan JS-L, Wong JP-M and Wang K-L (2023), Early Cretaceous volcanic-arc magmatism in the Dalat-Kratie Fold Belt of eastern Cambodia: implications for the lithotectonic evolution of the Indochina terrane.
Front. Earth Sci. 11:1110568.
doi: 10.3389/feart.2023.1110568

Early Cretaceous volcanic-arc magmatism in the Dalat-Kratie Fold Belt of eastern Cambodia: implications for the lithotectonic evolution of the Indochina terrane

J. Gregory Shellnutt[1]*, George S.-K. Ma[2], Jacky S.-L. Chan[3], Jean P.-M. Wong[4] and Kuo-Lung Wang[5]

[1]National Taiwan Normal University, Department of Earth Sciences, Taipei, Taiwan, [2]The Chinese University of Hong Kong, Jockey Club Museum of Climate Change, Shatin, NT, Hong Kong SAR, China, [3]ProjecTerra, Hong Kong, Hong Kong SAR, China, [4]The University of Hong Kong, Department of Earth Sciences, Pokfulam, Hong Kong SAR, China, [5]Academia Sinica, Institute of Earth Sciences, Taipei, Taiwan

Mesozoic granitic plutons are found throughout the Indochina terrane of eastern Cambodia and southern Vietnam. The granitic rocks range in age from Early Triassic (240 Ma) to Late Cretaceous (80 Ma) and record distinct tectonomagmatic periods associated with subduction of the Paleotethys and Paleo-Pacific oceans. Samples collected from the Snoul pluton, eastern Cambodia are composed of silicic and intermediate dioritic rocks, and basalt. The quartz diorites and diorites are magnesian, metaluminous, calcic to calc-alkalic, and similar to volcanic-arc granitoids whereas the basaltic rocks are compositionally similar to within-plate basalt. Zircon U-Pb geochronology and Lu-Hf isotopes and whole rock Sr-Nd isotopes show that the silicic rocks are Albian and isotopically juvenile (107.5 ± 0.3 Ma, 109.1 ± 0.4 Ma; $\varepsilon_{Hf}(t)$ = +7.0−+17.0; $^{87}Sr/^{86}Sr_i$ = 0.704313−0.707681; $\varepsilon_{Nd}(t)$ = +3.1−+4.9). Fractional crystallization modeling using a dioritic composition as the parental magma demonstrates that it is possible to generate the quartz diorite compositions under oxidizing (ΔFMQ +1) and hydrous (H_2O = 2 wt%) conditions suggesting that they are consanguineous. The isotopically juvenile nature of the dioritic rocks and their compositional similarity ($SiO_2 \geq 56$ wt%, $Al_2O_3 \geq 15$ wt%, Sr ≥ 400 ppm, Y ≤ 18 ppm, Yb ≤ 1.9 ppm) to adakitic rocks indicates that the parental magmas of the Snoul pluton were likely derived by partial melting of juvenile mafic basement rocks of the Indochina terrane. Moreover, Early Cretaceous plutonic rocks of Cambodia are isotopically distinct from plutonic rocks of similar age and tectonic setting from Vietnam suggesting that there could be a lithotectonic domain boundary within the Southern Indochina terrane. In contrast, the basaltic rocks likely record a temporally distinct period of magmatism associated with Late Cenozoic tensional plate stress.

KEYWORDS

Indochina terrane, volcanic-arc granite, mafic enclaves, Dalat-Kratie Belt, Early Cretaceous

Introduction

The Mesozoic Era was an important time for the lithospheric evolution of South, Southeast, and East Asia (Sone and Metcalfe, 2008; Hall, 2012; Hall, 2017; Wang et al., 2013; Hutchison, 2014; Metcalfe, 2017). During the Triassic to Cretaceous lithotectonic terranes derived from Gondwana (e.g., Qiangtang, West Myanmar, Sibumasu, Indochina) drifted across the Tethyan oceans and accreted to the southern Eurasian margin and cratons of China (Carter et al., 2001; Metcalfe, 2006; Metcalfe, 2013; Carter and Clift, 2008). Furthermore, the North China Block and South China Block amalgamated and subduction of the Paleo-Pacific plate beneath eastern Eurasia initiated periods of variably intense arc magmatism until the Late Cretaceous (Zhou et al., 2006; Li and Li, 2007; Faure et al., 2008; Lepvrier et al., 2008). Subsequently, during the Cenozoic, the India-Eurasia collision ushered in a period of regional horizontal and vertical tectonics across south and southeast Asia that led to the reorganization and displacement of the accreted terranes (White and Lister, 2012; Bouilhol et al., 2013; Schellart et al., 2019). Moreover, the secession of subduction-related magmatism in the east was followed by a period of crustal relaxation and the development of the proto-South China Sea (Zheng et al., 2019).

Of particular interest is the evolution of the Indochina terrane as it was affected by multiple collisional and accretionary events related to the subduction of the Paleotethys Ocean (Sone and Metcalfe, 2008; Hutchinson, 2014; Metcalfe, 2017; Faure et al., 2018; Wang et al., 2018; Tran et al., 2020; Waight et al., 2021). During the Early Triassic, the Indochina terrane collided and accreted to the South China Block whereas during the Late Triassic it was affected by collision and accretion of the Sukhothai and Sibumasu terranes (Lepvrier et al., 2008; Burrett et al., 2021; Jiang et al., 2021). Furthermore, the Paleo-Pacific plate subducted beneath the Indochina terrane beginning in the Early Cretaceous and was responsible for the generation of widespread Cordilleran Batholiths throughout the Dalat-Kratie Fold Belt of southern Vietnam and eastern Cambodia (Nguyen et al., 2004a; Nguyen et al., 2004b; Shellnutt et al., 2013; Cheng et al., 2019; Hennig-Breitfeld et al., 2021; Nong et al., 2021; Nong et al., 2022). The Dalat-Kratie Fold Belt is composed of Triassic to Cretaceous sedimentary rocks and volcano-plutonic rocks that are overlain by Quaternary basalt (Zaw et al., 2014). The granitic rocks are primarily of Cretaceous (130-75 Ma) ages, although Carboniferous (332 ± 5 Ma), Permian (277 ± 2 Ma), and Triassic (202 ± 0.4 Ma; 238 ± 0.3 Ma; 211 ± 1.7 Ma; 248.9 ± 2.4 Ma) mafic and silicic igneous rocks are also present in the region (Nguyen et al., 2004a; Nguyen et al., 2004b; Shellnutt et al., 2013; Cheng et al., 2019; Hennig-Breitfeld et al., 2021; Kasahara et al., 2021).

The Cretaceous rocks record two distinct periods of granitic magmatism related to the subduction of the Paleo-Pacific plate. The more voluminous, older (130–90 Ma) rocks are attributed to volcanic-arc magmatism and contemporaneous with the Late Yanshanian Orogeny of East Asia whereas the younger (<90 Ma) rocks are correlated with post-collisional magmatism (Nguyen et al., 2004a; Nguyen et al., 2004b; Shellnutt et al., 2013; Cheng et al., 2019; Hennig-Breitfeld et al., 2021; Kasahara et al., 2021). Located within the Dalat-Kratie Fold Belt of eastern Cambodia is the previously unstudied Snoul pluton. Rocks were collected from a surface exposure and mineral exploration drill core. The surface exposure is composed of quartz diorite and diorite whereas the drill core encountered basaltic dykes and dioritic enclaves within the host quartz diorite.

In this paper, we present *in situ* zircon U-Pb geochronology and Hf isotopes, whole rock geochemistry, and whole rock Sr-Nd isotopes of host rocks and enclaves collected from the surface and drill core of the Snoul pluton of eastern Cambodia. The results of this study are used to constrain the age of emplacement and the tectonomagmatic evolution of the host quartz diorite within the context of Mesozoic tectonics of the Indochina terrane. Moreover, we evaluate the relationship between the dioritic and basaltic enclaves to the host rocks in order to assess their petrogenetic relationship.

Geological Background

Present-day Southeast Asia is composed largely of terranes derived from the margin of eastern Gondwana (e.g., Hall, 2012; Hall, 2017; Metcalfe, 2013; Metcalfe, 2017; Usuki et al., 2013). Major terranes include South China, Indochina, Sibumasu, West Burma, East Malay, and West Sumatra (Figure 1) which travelled northwards from the southern hemisphere and accreted to the southern margin of Eurasia. Convergence is still ongoing today, as the Australian plate approaches northward *via* subduction beneath Sumatra, Java, and Timor. The long-term convergence in this region has resulted in multiple episodes of arc magmatism, ocean basin opening and closure, and mountain-building events. The resultant deformation zones and fold belts are important sites of mineral resources such as orogenic gold, porphyry copper, volcanic-hosted massive sulphide, and gemstone deposits (Zaw et al., 2014).

Of the Gondwana-derived fragments, the Indochina Block is one of the largest tectonic units in Southeast Asia, occupying much of Cambodia, Laos, Malaysia, Myanmar, Thailand, and Vietnam (Figure 1; Hutchinson, 2014; Metcalfe, 2017; Nakano et al., 2021). The Indochina Block is bounded to the northeast by the Ailaoshan–Song Ma suture and to the west by the Sukhothai–Chanthaburi arc and the Paleo-Tethys suture. The block is generally divided into several tectonic zones: the Truong Son Fold Belt (Laos and western Vietnam) and Kontum massif (central Vietnam) along its eastern margin, the Loei Fold Belt (western Cambodia, Thailand and eastern Myanmar) along the western margin and the Dalat–Kratie Fold Belt (eastern Cambodia and southern Vietnam) in the south (Hutchinson, 2014; Metcalfe, 2017; Burrett et al., 2021).

The Truong Son Fold Belt is composed of Ordovician–Carboniferous and Neoproterozoic–Silurian sedimentary rocks intruded by Permian-Triassic volcanic and intrusive rocks (Lepvrier et al., 2004; Burnett et al., 2021). The Kontum massif represents a metamorphic core of granulite facies rocks, with Nd depleted mantle model ages of 2.4-1.2 Ga (Lan et al., 2003) and an inherited U–Pb zircon core of 1.4 Ga (Nam et al., 2001). Subsequent deformation and metamorphic overprinting on the Truong Son and Kontum rocks suggests that the accretion of the Indochina Block to the Eurasia margin occurred during the Early Triassic (260-240 Ma; Carter et al., 2001; Lepvrier et al., 2004; Roger et al., 2007). The Loei Fold Belt is composed of a succession of carbonates and metamorphosed tuffaceous rocks, intruded or overlain by Silurian to Late Cenozoic igneous rock (Wang et al., 2018; Burrett et al., 2021; Shi et al., 2021).

The Dalat–Kratie Fold Belt is composed of a Precambrian basement, Triassic–Cretaceous sedimentary rocks, Cretaceous granitic rocks, and Cenozoic intraplate basaltic rocks (Nguyen et al., 2004a; Nguyen et al., 2004b). The Cretaceous granitoids can be subdivided into I-type and A-type (Nguyen et al., 2004a; Nguyen et al., 2004b; Shellnutt et al., 2013; Waight et al., 2021). The more widespread I-type Early Cretaceous granitic batholiths are related to the subduction of the Paleo-Pacific Ocean crust beneath Indochina and contemporaneous with Yanshanian magmatism along the coast of eastern China. The Late Cretaceous A-type granitic rocks that crop out

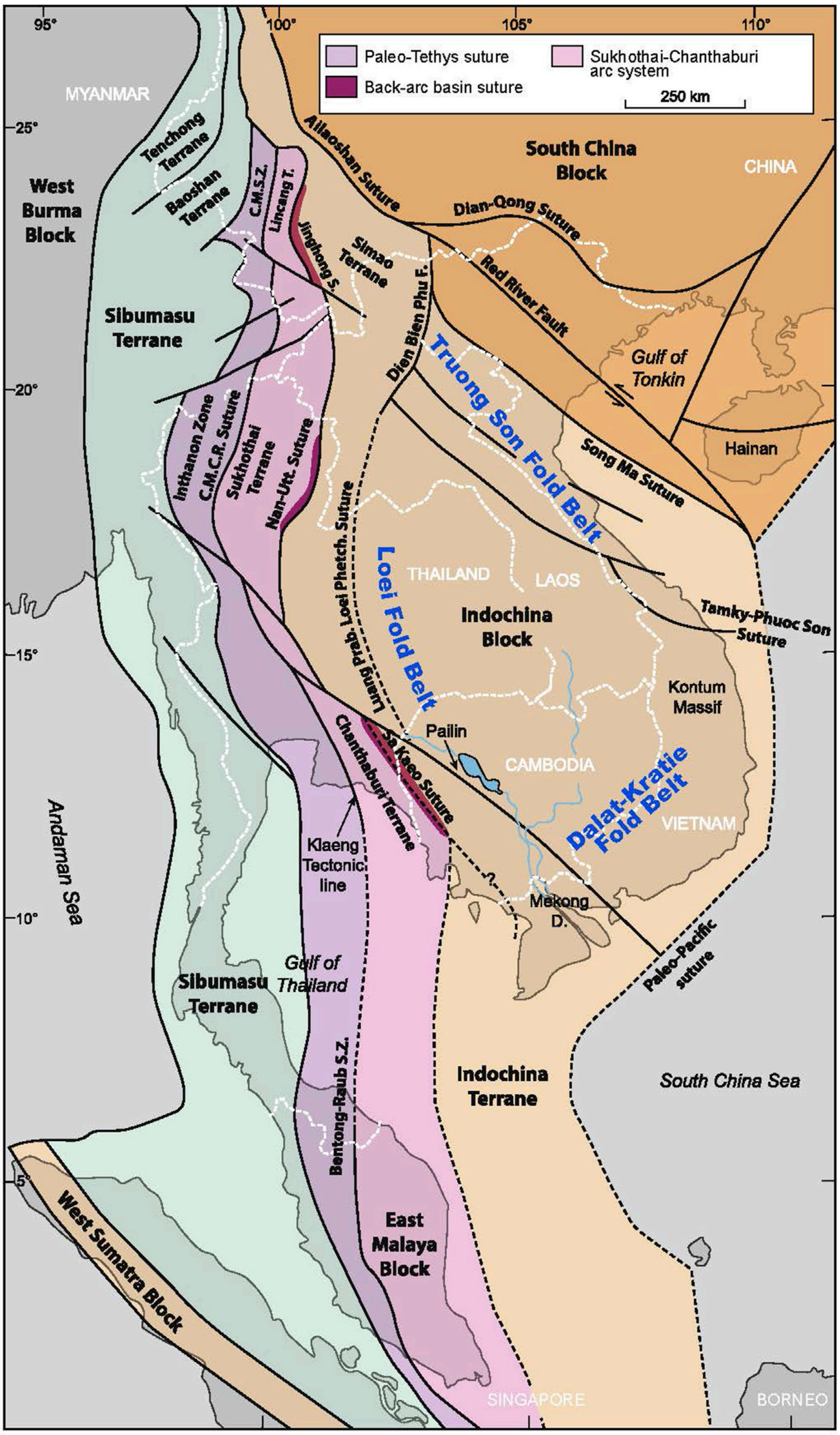

FIGURE 1
Tectonic subdivision of geological terranes of Southeast Asia showing the location of the Dalat-Kratie Fold Belt (modified from Metcalfe, 2017).

in southern Vietnam are interpreted to be related to post-collision extensional stress associated with trench retreat and slab rollback of the Paleo-Pacific Ocean (Zhou et al., 2006; Shellnutt et al., 2013; Cheng et al., 2019; Hennig-Breitfeld et al., 2021; Kasahara et al., 2021; Waight et al., 2021; Nong et al., 2022).

Sample locations

The present study focuses on the granitic rocks and enclaves of the Snoul pluton within the Dalat–Kratie Fold Belt of eastern Cambodia (Figure 2). The Snoul pluton is a newly discovered intrusion of the upper

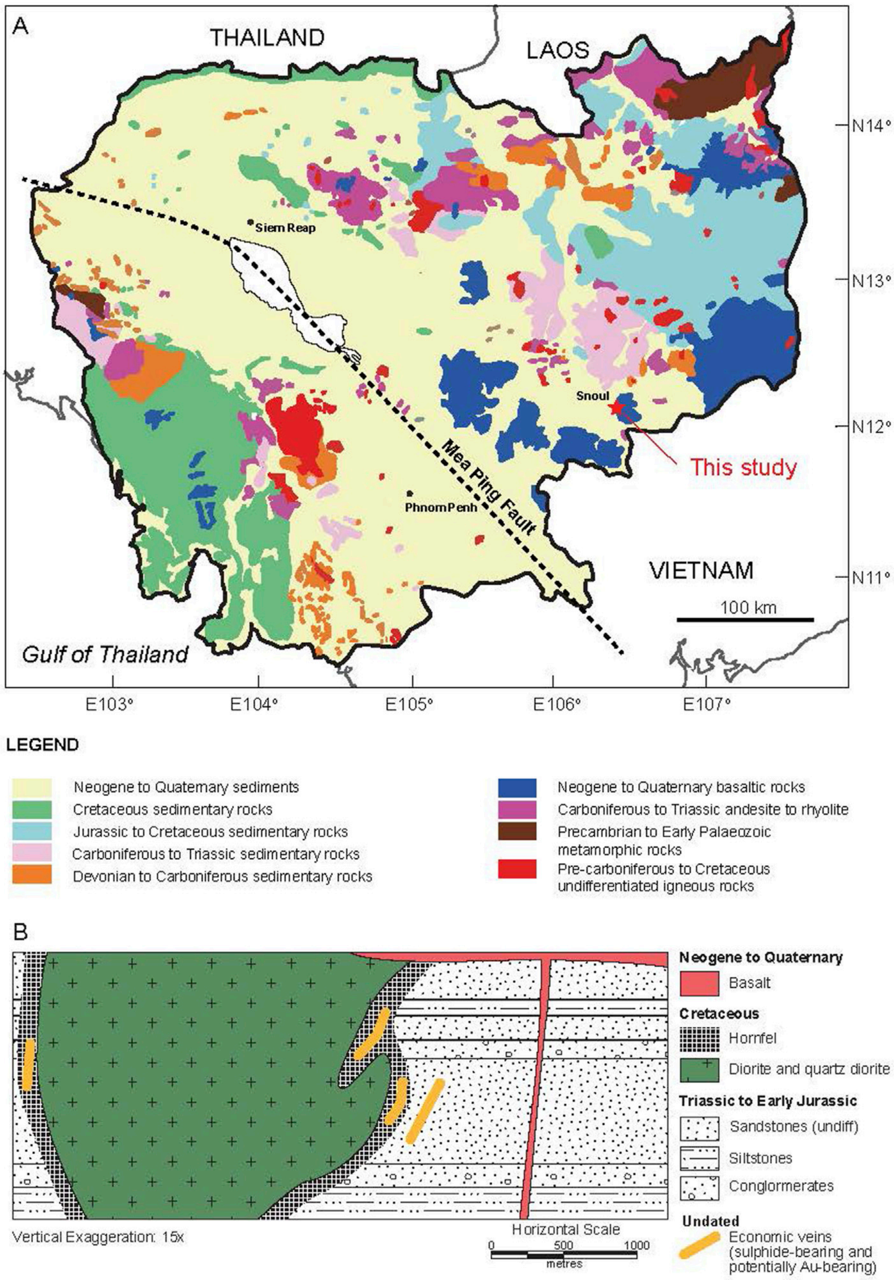

FIGURE 2
(A) Geological map of Cambodia showing the location of the Snoul pluton (modified from Kasahara et al., 2021). **(B)** Schematic cross-section of the region underneath the Snoul pluton (green) highlighting the stratigraphic relationships of various lithological units.

crust that intrudes Triassic–Early Jurassic sandstones, siltstones and conglomerates, although detailed field mapping of the pluton was not possible due to the widespread Quaternary sedimentary cover in the region (Figure 2B). Field occurrences, drill core logging, and geophysical surveys (e.g., airborne magnetic anomalies) were used by local exploration companies to interpret the extent of the pluton which is estimated to be 1.5–2 km in diameter. At least two varieties of quartz diorite were observed in the field, one finer-grained and the other coarser-grained, but with similar mineralogy. The best exposure can be found at 0647977 mE, 1328288 mN and its vicinities, where a fine–medium-grained dioritic body is intruded by aplite and mafic dykes (Figures 3A–C). Most of the samples (A15-series, A17-series) were selected from drill cores provided by Southern Gold (Cambodia) obtained from its 2009 drilling campaign (Figures 3C, D). The drill core samples were split diagonally with one-half taken for this study and the other half retained by Southern Gold (Cambodia). Other samples (O-series) were collected from the few exposed surface outcrops.

Petrography

Quartz diorite

The quartz diorite host rocks (A15.2, A17.1ah, A17.3b, A17-7-HA, A17-14-h, O27b, O52B) were collected from the surface and the drill core. The rocks are coarse grained and granular with the surface

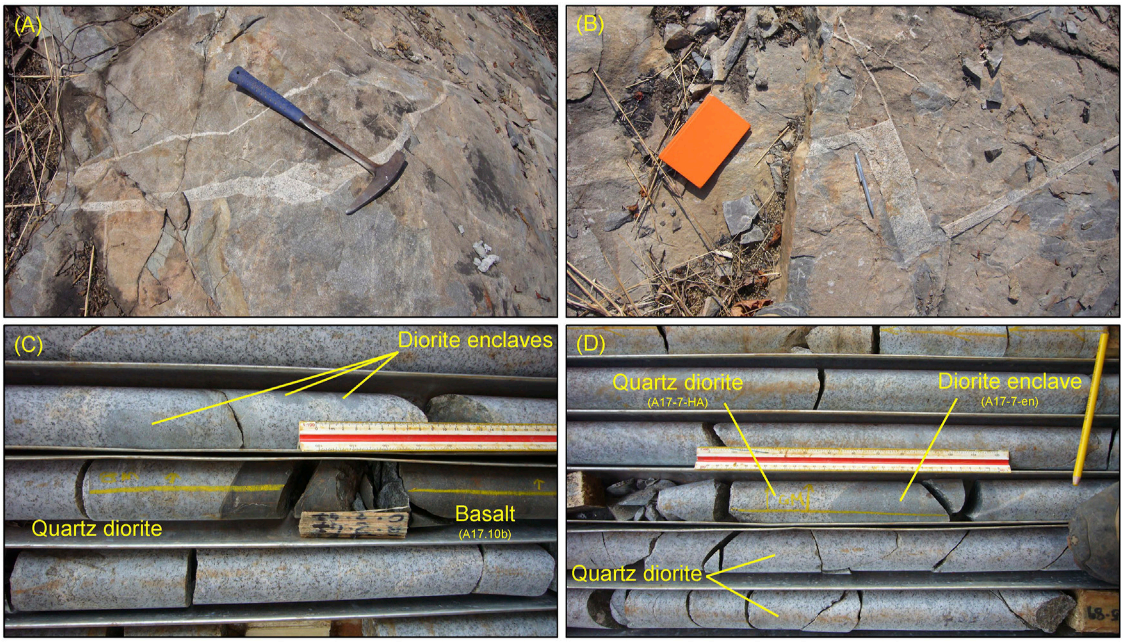

FIGURE 3
Field and drill hole photos of the Snoul pluton. **(A, B)** Fine to medium-grained diorite intruded by a coarse-grained dioritic dyke, demonstrating both **(A)** diffusive and **(B)** brittle, crack-filling fashion of dyking. **(C, D)** Diorite enclaves (irregular- to rounded shape) and basalts in a quartz diorite host rock intersected by drill hole A17 of the Snoul pluton.

samples tending to be more altered than those from the drill core. The rocks are composed of plagioclase (45–50 vol%), amphibole (~35 vol%), quartz (5–15 vol%), biotite (≤5 vol%), and Fe-Ti oxide minerals (≤5 vol %) with accessory amounts (≤1 vol% each) of apatite, zircon, and titanite. Plagioclase is euhedral to subhedral and with straight crystal edges (Figures 4A, B). The larger plagioclase crystals tend to have oscillatory zonation, but the smaller crystals tend to display polysynthetic twinning with a few showing albite twinning. All plagioclase crystals are altered by saussurite, although the extent of alteration can range significantly between different samples. Amphibole (hornblende) is the primary mafic silicate mineral in the rock and is euhedral to anhedral (Figure 4A). Similar to the plagioclase crystals, there are larger (1–3 mm) euhedral crystals (~5 vol%), but most are smaller (<1 mm) and interstitial to the plagioclase. Most of the amphibole crystals are altered by chlorite and/or biotite. The quartz crystals are subrounded and interstitial to the plagioclase and amphibole. The amount of quartz can vary between samples and is typically 5–15 vol%. Euhedral to subhedral biotite is common but its abundance can vary between samples (≤5 vol%). The biotite crystals are tan brown to brown in colour with some crystals having zircon inclusions. Under reflected light, it appears that nearly all of the opaque minerals are magnetite and ilmenite as sulphide minerals were not identified. The opaque minerals are euhedral to subhedral with most having cubic or subrounded shapes (Figure 4A).

Diorite

The diorite rocks (host = A17-8-h, O05c, O20, O27a; enclaves = A17.4b, A17-7-en, A17-8-EN, A17-14-h) were collected from the surface exposure and the drill core. The rocks are phanerocrystalline with some samples having medium to coarse grained textures whereas others are medium to fine grained. In general, the surface samples tend to be more altered than those from the drill core. The mineralogy and textures of the diorites are similar to the quartz diorites, but they have less quartz and biotite (Figures 4C, D). The rocks are primarily composed of plagioclase (50–55 vol%), amphibole (35–40 vol%), and opaque (Fe-Ti oxide minerals) minerals (~5 vol%) with accessory amounts (≤1 vol% each) of quartz, biotite, apatite, zircon, and titanite.

Mafic dykes

The mafic rocks (A15.1b, A17.1b, A17.9, A17.10b) have similar textures and mineralogy and are relatively fresh, but show signs of zeolite facies alteration (Figures 4E, F). The rocks are porphyritic and seriate and composed mostly of plagioclase (50–55 vol%) and clinopyroxene (35–40 vol%) with subordinate amounts of ilmenite/magnetite (5–10 vol%), and olivine (~5 vol%). The plagioclase crystals are mostly euhedral and have lath shapes of similar size. The clinopyroxene (augite) crystals are light brown in colour, subhedral to euhedral in shape. The olivine crystals are euhedral to anhedral (sub-round) and mostly appear as larger phenocrysts. The opaque minerals are euhedral to subhedral with cubic shapes. The basaltic rocks are likely dykes rather than xenoliths as the chilled margin with the host rock was observed (Figures 4G, H). The contact between the quartz diorite host and the basalt is sharp, but there appears to be reaction/transition zone as the contact region changes from brown to dark brown (Figure 4G). The transition zone is aphyric with occasional xenocrysts of quartz and feldspar from the host rock. Farther from the contact, the xenocrysts are absent and the basaltic rock is porphyritic with euhedral to subhedral phenocrysts of olivine and plagioclase microlites (hyalopilitic).

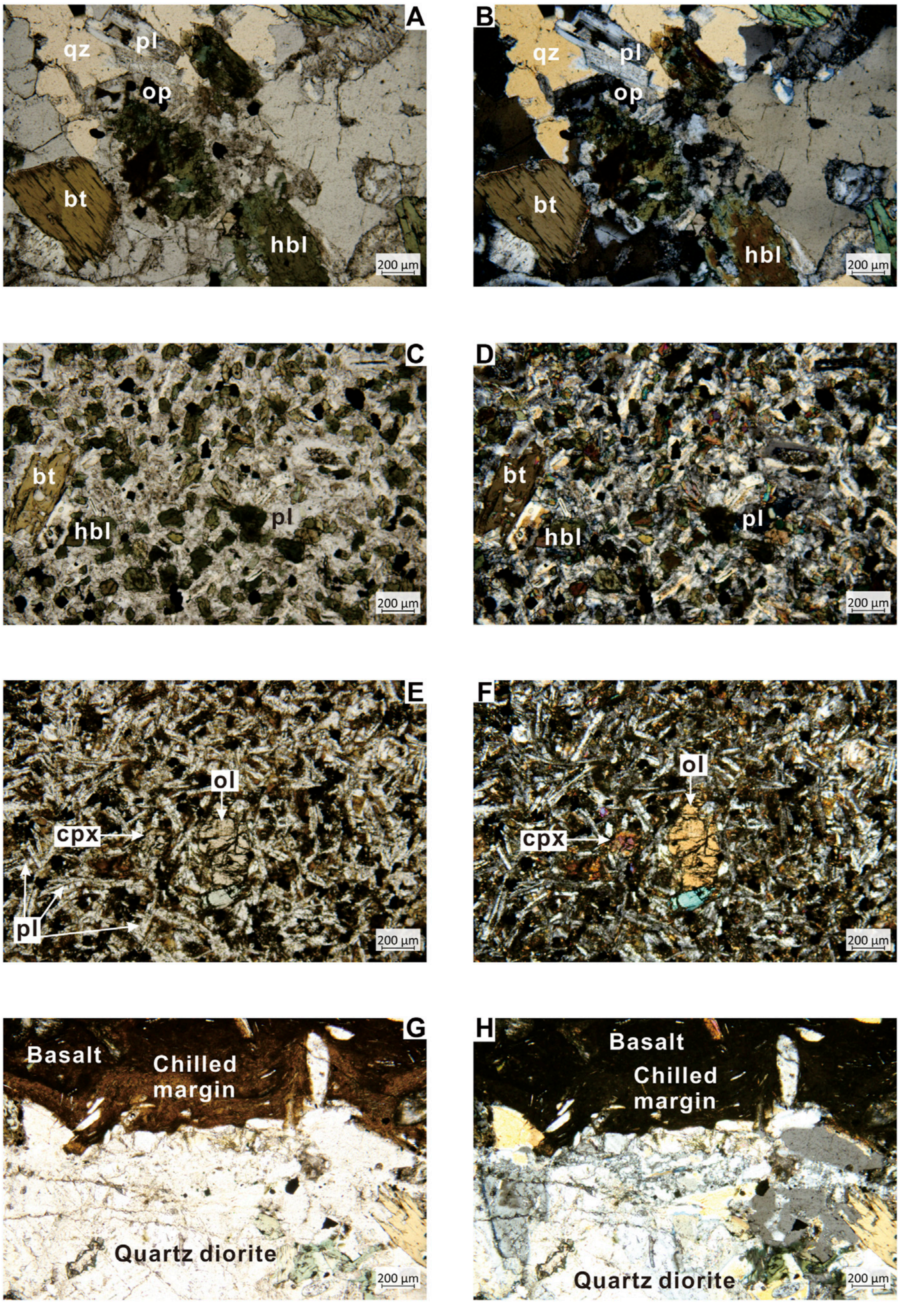

FIGURE 4
Photomicrographs of the rocks of the Snoul pluton. **(A)** Plane polarized light and **(B)** crossed polarized photos of the quartz diorite (A17-3a). **(C)** Plane polarized light and **(D)** crossed polarized photos of a diorite enclave (A17-13). **(E)** Plane polarized light and **(F)** crossed polarized photos of a basaltic rock (A15-1b). **(G)** Plane polarized light and **(H)** crossed polarized photos of the chilled margin between the quartz diorite and basalt. Symbols: qz = quartz, bt = biotite, pl = plagioclase, op = opaque, hbl = hornblende, ol = olivine, cpx = clinopyroxene. Whole rock geochemical data were not measured for samples A17-3a or A17-13.

Materials and Methods

Zircon U-Pb and Lu–Hf isotopic analyses

In situ U-Pb and Lu-Hf isotopic analyses presented in this study were performed using a Nu Plasma HR multi-collector inductively coupled plasma mass spectrometer (MC-ICPMS; Nu Instruments, UK) equipped with an ArF excimer 193 nm laser ablation system (RESOlution M-50, Resonetics LLC, USA), housed at the Department of Earth Sciences, The University of Hong Kong, HKSAR. A modified collector block of the MC-ICPMS contains 12 Faraday collectors and 4 ion counting detectors dispersed on the low mass side of the array, allowing simultaneous acquisition of ion signals ranging from mass ^{204}Pb to ^{238}U. A spot diameter of 30 μm, pulse rate of 6 Hz and energy density of 15 J/cm^2 were used. Ablation time was 40 s, resulting in pits 20–30 microns deep. Instrument parameters can be referred to Xia et al. (2011). The standard zircon 91500 (Wiedenbeck et al., 1995) and GJ-1 (Jackson et al., 2004) were used for calibration. Off-line data reduction was performed by the software *ICPMSDataCal. Version 7.2* (Liu et al., 2010). Ages were calculated using ISOPLOT/Excel version 3.6 (Ludwig, 2008). The results are presented in Supplementary Tables S1, S2 where the isotopic ratios and ages are given with 1 sigma error.

The zircon Hf isotopes were analyzed on the same spots as those with a concordant U-Pb age. The Hf isotopic data reported in this study were obtained with a beam diameter of 55 μm, pulse rate of 6 Hz and energy density of 15 J/cm^2. Each analytical spot was subjected to 40 ablation cycles, resulting in pits 30–40 μm deep. Atomic masses 172 to 179 were simultaneously measured in static-collection mode. Isobaric interference of ^{176}Yb on ^{176}Hf was corrected against the ^{176}Yb/^{172}Yb ratio of 0.5886 (Chu et al., 2002). Interference of ^{176}Lu on ^{176}Hf was corrected by measuring the intensity of the interference-free ^{175}Lu isotope and using a recommended ^{176}Lu/^{175}Lu ratio of 0.02655 (Machado and Simonetti, 2001). External calibration was made by measuring zircon standard 91,500 (^{176}Hf/^{177}Hf = 0.282275 ± 0.000011) for the unknown samples during the analyses to evaluate the reliability of the analytical data and GJ-1 has been used for monitoring the data quality which yielded a weighted mean ^{176}Hf/^{177}Hf ratio of 0.282008 ± 0.000001 (Supplementary Table S3).

The measured ^{176}Lu/^{177}Hf and ^{176}Lu/^{177}Hf ratios and a^{176}Lu decay constant of 1.865 x $10^{-11}a^{-1}$ as reported by Scherer et al. (2001) were used to calculate the initial ^{176}Hf/^{177}Hf ratios. Calculations of $\varepsilon_{Hf}(t)$ values were based on the chondritic values of ^{176}Hf/^{177}Hf and ^{176}Lu/^{177}Hf as reported by Blichert-Toft and Albarède (1997). The mantle extraction model age (T_{HfDM}) was calculated using the measured ^{176}Lu/^{177}Hf of the zircon, but this only provides a minimum age for the source material of the magma from which the zircon crystallized. Therefore, "crustal" model ages T_{Hfc} were calculated (Supplementary Table S3), which assume that the parental magma of the zircons was produced from average continental crust, but was ultimately derived from the depleted mantle. A ratio of 0.015 most realistically reflects the ^{176}Lu/^{177}Hf ratio of our samples.

Wavelength dispersive X-ray fluorescence

Three grams (3.0000 ± 0.0005 g) of each sample was added to a ceramic crucible of known mass (+lid) and placed in an oven at 105°C for 3 h. After the initial heating step, the powders were cooled to ambient temperature inside a desiccator for ~15 min before they were weighed. The samples were then baked to peak temperature at 900°C (held for 10 min) in a high temperature furnace before cooling. The samples were then cooled in a desiccator until reaching ambient temperature. Each sample was weighed for a final time and the loss on ignition was calculated from the masses obtained from the low and high temperature cycles. Six grams (6.0000 ± 0.0005 g) of lithium metaborate was added to each sample (0.6000 ± 0.0005 g) at a ratio of 10:1 and fused to produce a glass disc using a Claisse M4 fluxer. The major elements were measured by wave-length dispersive X-ray fluorescence using Panalytical Axios^{mAX} at the XRF Laboratory, Department of Earth Sciences, National Taiwan Normal University. Standard reference materials measured during the study include: BIR-1a, BCR-2, and AVG-2a (Supplementary Table S4).

Inductively coupled plasma mass spectrometry

Trace elements were measured using an Agilent 7500cx inductively coupled plasma mass spectrometer (ICP-MS) at National Taiwan University, Taipei, Taiwan. Approximately 50–100 mg of each sample powder was dissolved in a Teflon beaker using a combination of HF, HNO_3, and HCl. Each sample was heated in closed beakers with HF and HNO_3 for at least 48 h and then dried. After drying, 2 mL of 6 N HCl was added to each sample and then left to dry. This step was followed by the addition of 2 mL of 1 N HCl to each sample then the solution was centrifuged. The supernatant was extracted and then placed into a new beaker. If solid residue remained in the beaker after extraction, then the procedure was repeated until the powder was fully digested. Samples were diluted using 2% HNO_3 and an Rh and Bi spike was added for the internal standard. The standard reference materials measured for the trace elements of this study are AGV-2 (andesite), BCR-2 (basalt), and DNC-1 (dolerite) (Supplementary Table S4).

Thermal ionization mass spectrometry

Whole rock Sr and Nd isotopes were measured at the Institute of Earth Sciences, Academia Sinica, Taipei (Supplementary Table S5). Approximately 75 mg of sample powder was dissolved using a mixture of HF and HNO_3 at 120°C for 48 h, then taken to dryness followed by dissolution in 2 mL 4 N HCl. Separation and purification of Sr and Nd were achieved using a 3-column technique. The first column was contained 0.2 mL Sr spec resin (manufactured by Eichron Industries, Inc.) to collect the Sr fraction using HNO_3 as eluent. The elution was then passed through the second column containing 2.5 mL cation exchange resin (Bio Rad AG50W-X8, 100–200 mesh) to isolate the rare Earth elements using HCl as eluent. The third column used for Nd separation contained 1 mL Ln-B25-A (Eichrom) resin, covered on top by a thin layer of anion exchange resin (Bio Rad AG1-X8, 200–400 mesh), using HCl as eluent.

Strontium was loaded on a single Ta filament and compositional analysis was performed using 7-collector Finnigan MAT-262 thermal ionization mass spectrometer in dynamic mode. Neodymium loaded on a double Re filament and the isotopic measurement was analyzed using 9-collector Thermo Fisher Scientific Triton thermal ionization mass spectrometer with static mode for automatic run. The isotopic ratios were corrected for mass fractionation by normalizing to ^{86}Sr/^{88}Sr = 0.1194 and ^{146}Nd/^{144}Nd = 0.7219. At the time of analysis, the NBS-987 Sr standard yielded an average value of ^{87}Sr/^{86}Sr = 0.710249 with a long-term reproducibility of 0.000045 (2σ) and the JMC Nd standard gave an average of ^{143}Nd/^{144}Nd = 0.511813 with a long-term reproducibility of 0.000009.

Results

In situ zircon U-Pb ages

Twenty-six zircons were analyzed from sample O05c (diorite). Zircon grains range in size from ~50 μm to ~300 μm in length and have euhedral (prismatic to equant) to subhedral (fragmented to sub-round) shapes. Nearly all zircons show igneous (oscillatory) zonation whereas very few have core-rim structures (Corfu et al., 2003). All zircons yielded ages that were 92% concordant or better, however we only select zircons with ≥97% concordance to interpret their emplacement age (Supplementary Table S1). The ^{206}Pb/^{238}U ages revealed a bimodal distribution of ~111 Ma and ~107 Ma. Five

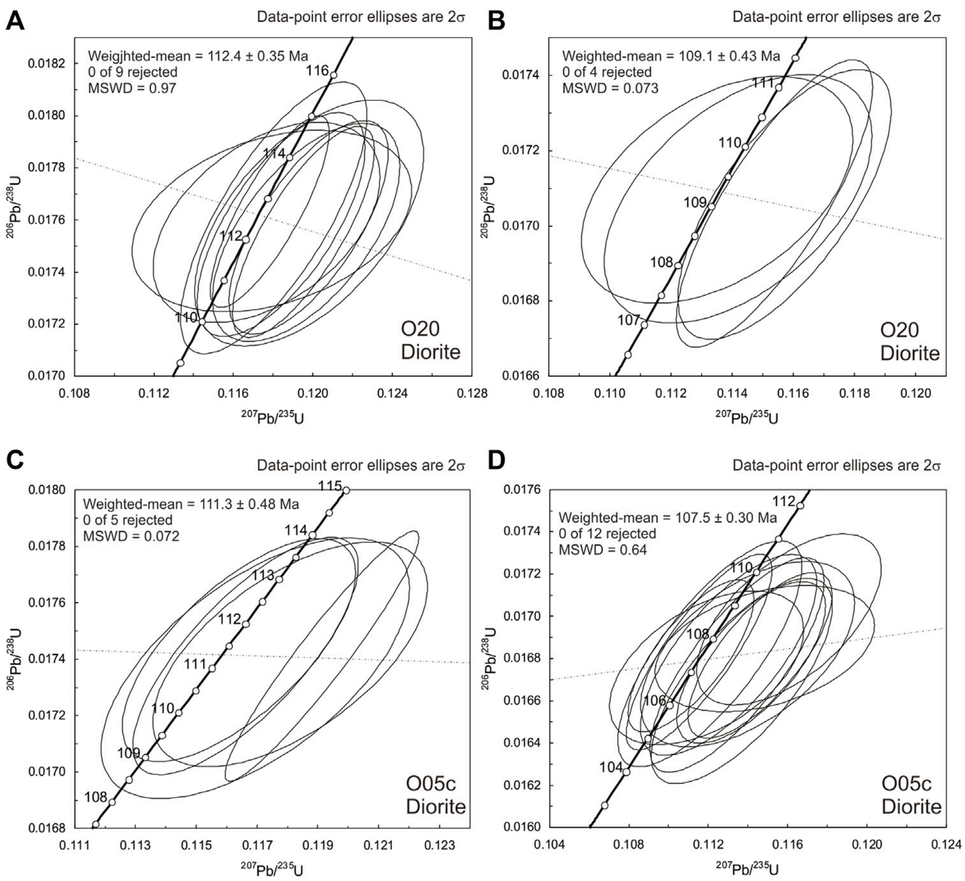

FIGURE 5
(A) Concordia diagram with the weighted-mean age of the older (inherited) population of zircon U-Pb data from sample O20. **(B)** Concordia diagram with the weighted-mean age of the younger population (emplacement age) of zircon U-Pb data from sample O20. **(C)** Concordia diagram with the weighted-mean age of the older (inherited) population of zircon U-Pb data from sample O05c. **(D)** Concordia diagram with the weighted-mean age of the younger (emplacement age) population of zircon U-Pb data from sample O05c.

zircons yielded an intercept age of 111.3 ± 1.8 Ma and weighted-mean $^{206}Pb/^{238}U$ age of 111.3 ± 0.5 Ma which we interpret as an inheritance age (Figure 5A). The majority of zircons (12) yielded an intercept age of 107.4 ± 1.0 Ma and weighted-mean $^{206}Pb/^{238}U$ age of 107.5 ± 0.3 Ma which we interpret as the emplacement age (Figure 5B). The older group of zircons (~111 Ma) do not show significantly different internal structures (i.e., core-rim structures) nor are their crystal shapes significantly different from the younger (~107 Ma) group of zircons.

Thirty-eight zircons were analyzed from sample O20 (diorite), however only twenty-six zircons with ≥97% concordance are considered for the emplacement ages (Supplementary Table S2). Zircon grains range in size from ~40 µm to ~400 µm in length and have euhedral (prismatic to equant) to subhedral (fragmented to sub-round) shapes. The zircons are morphological similar to those from sample O05c. The $^{206}Pb/^{238}U$ ages range from ~106 Ma to ~577 Ma with the majority (9) of ages around ~112 Ma. The nine zircons yielded an intercept age of 112.6 ± 1.4 Ma with a weighted-mean age of 112.4 ± 0.4 (Figure 5C). Four zircons with ≥97% concordance yielded an intercept age of 109.2 ± 1.3 Ma and weighted-mean $^{206}Pb/^{238}U$ age of 109.1 ± 0.4 Ma which we interpret as the emplacement age as they are within the uncertainty of the ages of O05c (Figure 5D). The inherited zircons with ≥97% concordance are mostly Carboniferous to Permian (258–335 Ma), but there are single zircon ages of ~106 Ma, ~114 Ma, ~118 Ma, and ~577 Ma. Much like sample O20, there does not appear to be significantly different internal structures or crystal shapes between the two groups of Cretaceous zircons. However, the older inherited zircons (i.e., >250 Ma) tend to have irregular to rounded shapes.

In situ zircon Hf isotopes

Hafnium isotopes were measured on the same zircon spot locations as the U-Pb ages of samples O20 and O05c. Not all zircons could be analyzed for Hf isotopes due to the limited amount of material left after ablation for U-Pb dating. The dataset can be found in the Supplementary Table S3. The depleted mantle lines in Figure 6 are defined by present-day $^{176}Hf/^{177}Hf$ = 0.28325 and $^{176}Lu/^{177}Hf$ = 0.0384 (Griffin et al., 2000).

The magmatic zircons (12) from sample O20 yielded initial $^{176}Hf/^{177}Hf(t)$ ratios from 0.283048 to 0.283186 with $\varepsilon_{Hf}(t)$ values ranging from +12.1 to +17.0. The meaningful T_{DM1} ages range from 123 Ma to 291 Ma whereas the T_{DM2} ages range from 141 Ma to 543 Ma. In comparison, the inherited (296–335 Ma) zircons (5) have initial $^{176}Hf/^{177}Hf(t)$ ratios from 0.282675 to 0.283025 and $\varepsilon_{Hf}(t)$ values ranging

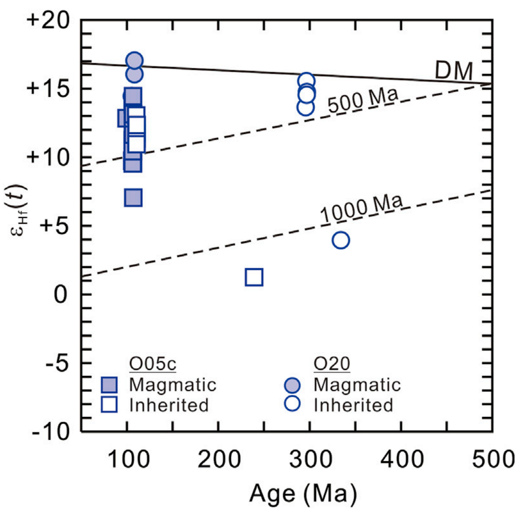

FIGURE 6
Zircon Hf isotopic evolution of the diorites (O05c, O20) from the Snoul pluton. The evolution curves (dashed lines) are calculated assuming Lu/Hf crustal value of 0.015 (Griffin et al., 2004; Chauvel et al., 2008). DM = depleted mantle.

from +3.9 to +15.5. The T_{DM1} ages range from 313 Ma to 813 Ma whereas the T_{DM2} ages range from 341 Ma to 1,490 Ma.

Twenty-two magmatic zircons from sample O05c yielded initial $^{176}Hf/^{177}Hf(t)$ ratios from 0.282904 to 0.283113 with corresponding $\varepsilon_{Hf}(t)$ values from +7.0 to +14.4. The T_{DM1} ages range from 194 Ma to 493 Ma whereas the T_{DM2} ages range from 319 Ma to 1,040 Ma. There is one inherited zircon (240 Ma). It has an initial $^{176}Hf/^{177}Hf(t)$ ratio of 0.282657 and $\varepsilon_{Hf}(t)$ value of +1.2 and T_{DM1} and T_{DM2} ages of 830 Ma and 1,688 Ma.

Major and trace elemental geochemistry

The SiO_2 contents of the host rocks range from ~55.7 to ~71.6 wt% with nearly all ANCK values (mol. Al_2O3/[mol. $CaO+Na_2O+K_2O$]) between 0.87 and 1.01 and alkali-alumina (mol. [Na+K]/mol. Al) values <1 (Figures 7A, B). According to the scheme of Frost et al. (2001), the rocks classify as magnesian (FeOt/FeOt+MgO = 0.65–0.71) and calcic (Figures 7C, D). Magnesian, metaluminous, calcic rocks are considered to be typical of the outboard portions of Cordilleran Batholiths (i.e., volcanic-arc granites). Sample A15.2 has very low Na_2O and K_2O contents and consequently has a very high ANCK value (~1.9). However, this sample is altered and it is likely that the alkali metals were mobilized (L.O.I. = 3.21 wt%). Nonetheless, for the exception of A15.2, all rocks are sodic (K_2O/Na_2O = 0.28–0.71) and their Mg# ([mol Mg/(mol Mg+tFe^{2+})]× 100) are 42.1–49.4 (Figures 7E, F). The loss on ignition (L.O.I.) values, for the exception of A15.2, are ≤0.51 wt% and indicate that the rocks did not undergo significant post-emplacement hydrothermal/deuteric alteration.

The host rocks have uniformly low concentrations of transition metals (Sc = 5.4–16.8 ppm), V = 93.6–170.6 ppm, Cr = 6–19 ppm, Co = 8.5–16.3 ppm, Ni = 4–8 ppm, Cu = 4.9–34.7 ppm, Zn = 16.7–55.3 ppm). The large ion lithophile element (LILE) concentrations are more variable (Rb = 0.9–84.9 ppm, Sr = 77–679 ppm, Cs = 0.12–2.3 ppm, Ba = 34–538 ppm). Similar to the LILE, the high field strength elements are variable (Zr = 22–108 ppm, Nb = 3.1–4.8 ppm, Y = 9.3–23.5 ppm, Hf = 0.78–2.68 ppm, Ta = 0.27–0.37 ppm, Th = 2.6–6.4 ppm, U = 1.1–1.9 ppm). The mid-ocean ridge basalt normalized incompatible patterns of the rocks are broadly similar, although there is some variability in the Rb–Ba and Hf–Zr concentrations (Figure 8A). All rocks have similar chondrite normalized rare Earth element patterns (Figure 8B). The rocks are light rare Earth element (REE) enriched with high La_N/Sm_N (1.9–3.3) and flat to bowl shaped middle to heavy REEs (Gd_N/Yb_N = 1.1–1.6) patterns. The Eu/Eu* values [2*Eu_N/(Sm_N+Gd_N)] are 0.93–1.09.

The four dioritic enclaves have intermediate compositions with SiO_2 ranging from 54.8–57.6 wt% and Na_2O+K_2O wt% equal to 5.2–5.6 wt% (Figure 7A). The enclaves are metaluminous, magnesian, and alkali-calcic (Figures 7B–D). The Fe_2O_3t ranges from 7.5–8.9 wt% and MgO from 3.9–5.0 wt% with the Mg# ranging from 46.6–53.6. The TiO_2 (0.65–0.68 wt%) and MnO (<0.25 wt%) contents are low and the CaO is ~7.5–7.8 wt%. The transition metals decrease with increasing SiO_2 contents, although some elements have limited variability (Sc = 14.1 and 21.9 ppm, V = 190 and 195 ppm, Cr = 18 and 38 ppm, Co = 16 and 17.5 ppm, Ni = 10 and 12 ppm, Cu = 22.4, and 38.4 ppm, Zn = 38.9–44.5 ppm). The mid-ocean ridge ocean basalt normalized incompatible element patterns are similar to the host rocks with enriched patterns of Cs, Rb, Ba, Th, and U with a depletion of Nb and relatively flat La–Nd patterns and flat but lower concentrations of Hf–Y with a positive anomaly of Sm (Figure 8C). The enclaves have light REE-enriched patterns with $(La/Yb)_N$ and $(La/Sm)_N$ ratios of 4.9–5.0 and 2.4. The rocks do not have negative Eu anomalies with Eu/Eu* ratios from 0.97–0.98 (Figure 8D). Furthermore, the rocks tend to have bowl shape patterns as the middle rare Earth elements (Dy–Er) are flat and the heavy rare Earth elements (Tm–Lu) are slightly higher.

The four basaltic rocks have SiO_2 ranging from 48.7–50.6 wt% and Na_2O+K_2O wt% equal to 4.2–5.4 wt% (Figure 7A). There is a distinct SiO_2 gap between the basaltic (~50.5 wt%) rocks and dioritic (~54.8 wt%) enclaves (Figures 7A, F). The basalts are mildly alkaline with alkalis (Na_2O+K_2O) increasing with increasing SiO_2 contents. The Fe_2O_3t ranges from 9.6–11.2 wt% and MgO from 4.9–9.1 wt% with the Mg# ranging from 50.1–61.7. The TiO_2 (1.5–1.6 wt%) and MnO (<0.20 t.%) contents are low. The Al_2O_3 ranges from 15.3–18.2 wt%, and CaO from 9.4–10.6 wt%. The transition metals generally decrease with increasing SiO_2 contents, although some elements have limited variability (Sc = 7.9–10.1 ppm, V = 219–224 ppm, Cr = 16–354 ppm, Co = 28.7–48.9 ppm, Ni = 24–205 ppm, Cu = 45.1–58.6 ppm, Zn = 81.5–111.7 ppm). The mid-ocean ridge ocean basalt normalized incompatible element patterns show low Cs and Rb concentrations and declining concentrations from Ba to Y (Figure 8E). The basalts have chondrite normalized light REE-enriched patterns with $(La/Yb)_N$ and $(La/Sm)_N$ ratios between 11.2 and 13.2 and 2.7–3.1. The rocks do not have significant negative Eu anomalies with Eu/Eu* ratios from 0.93–0.96 (Figure 8F).

Sr-Nd isotope geochemistry

Five samples were selected for Sr and Nd isotopic analysis (Supplementary Table S5). The initial isotopic ratios of the diorites and quartz diorites were calculated based on the U-Pb ages of this study (107 Ma) whereas the initial isotopic ratios of the basaltic rocks are thought to be contemporaneous with the adjacent Neogene–Quaternary volcanic rocks and an age of 10 Ma was

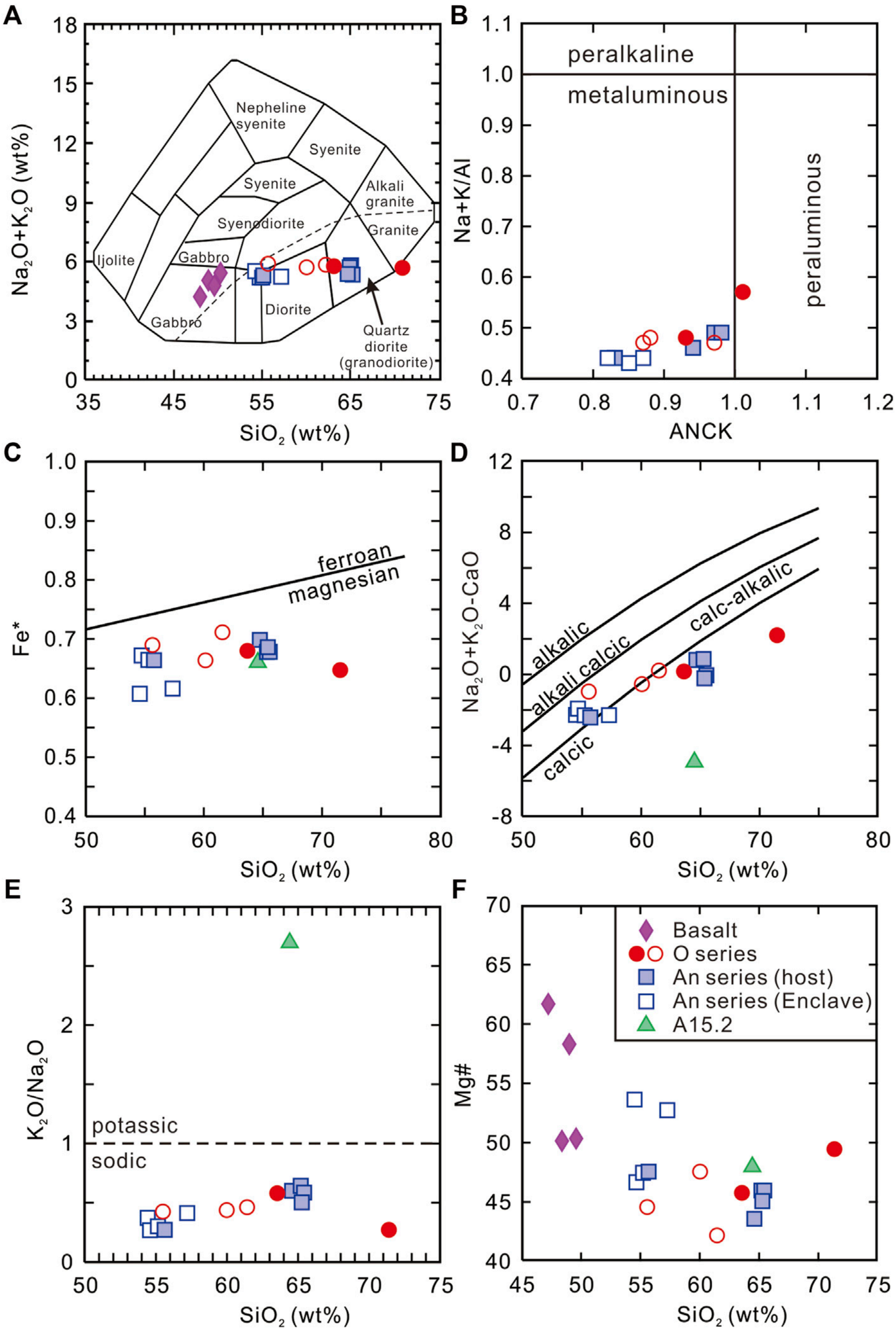

FIGURE 7
Chemical classification of the rocks from the Snoul pluton. **(A)** $Na_2O + K_2O$ (wt%) vs. SiO_2 (wt%) classification of rocks (Cox et al., 1979). **(B)** Alkali index (mol. Na + K/mol. Al) versus aluminum saturation index (ASI = mol. Al/mol. Ca + Na + K). Classification of the quartz dioritic and dioritic rocks using **(C)** the Fe* [(FeOt/(FeOt + MgO)] value and **(D)** the modified alkali-lime index ($Na_2O + K_2O$-CaO) vs. SiO_2 (wt%) of Frost et al. (2001). **(E)** K_2O/Na_2O vs. SiO_2 showing the sodic nature of the rocks. **(F)** Mg# vs. SiO_2 (wt%) of the mafic and silicic rocks from the Snoul pluton.

assumed (Nguyen and Flower, 1998). The initial $^{87}Sr/^{86}Sr$ ratios of the granitic rocks range from 0.704313 to 0.707681 (Figure 9). The initial $^{143}Nd/^{144}Nd$ ratios range from 0.512660 to 0.512750 for the granitic samples. Their $\varepsilon_{Nd}(t)$ values, using $^{147}Sm/^{144}Nd$ of 0.1967 and a $CHUR_{today}$ value of 0.512638, correspond to +3.1– +4.9 (Figure 9). The depleted mantle model ages (T_{DM}) range from 598 Ma to 847 Ma. The lone basalt sample has an initial $^{87}Sr/^{86}Sr$ ratio of 0.703978, an $\varepsilon_{Nd}(t)$ value of +4.2, and T_{DM} age of 513 Ma.

Discussion

Age of the Snoul pluton and its regional correlation

The zircon U-Pb geochronology results of the surface rocks yielded Albian ages (O05c = 107.5 ± 0.3 Ma; O20 = 109.1 ± 0.4 Ma). Moreover, sample O20 has inherited zircons that range in

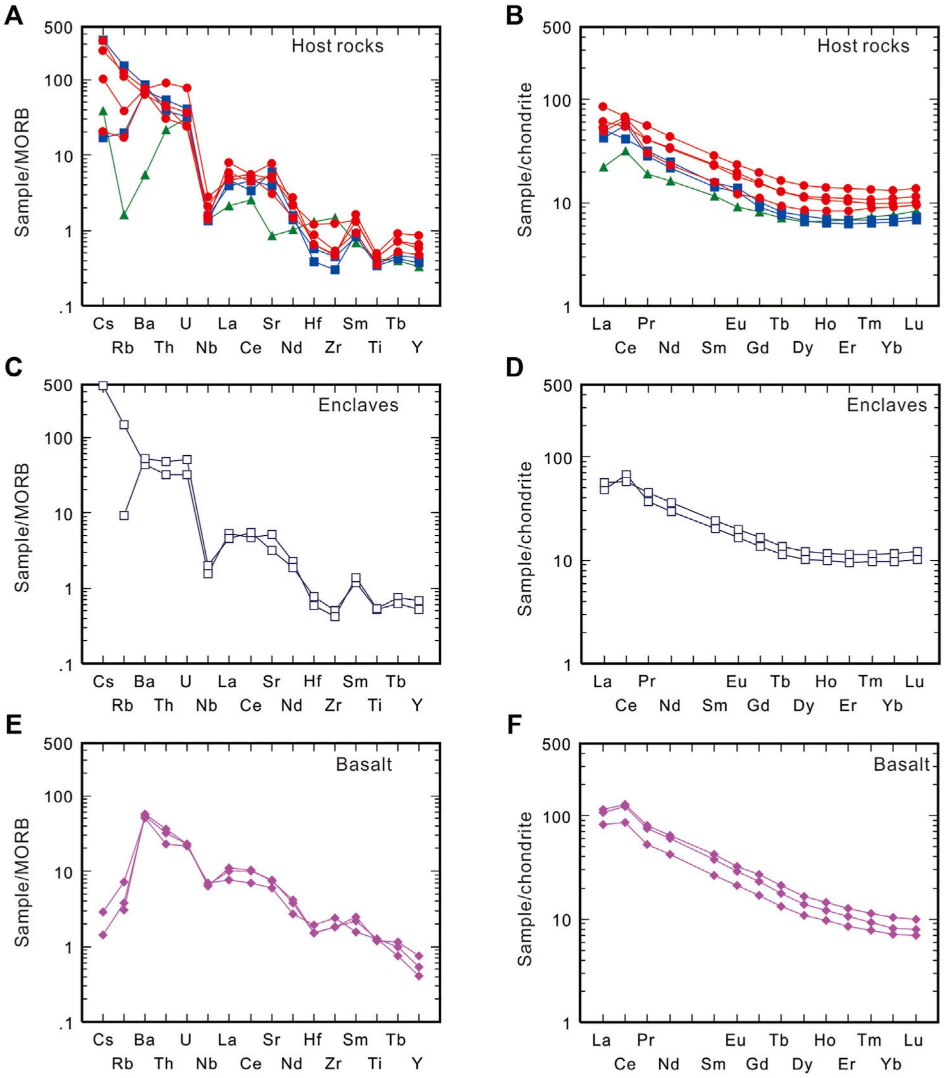

FIGURE 8
Mid-ocean ridge basalt (MORB) normalized incompatible element of the **(A)** host quartz dioritic and dioritic rocks, **(C)** the dioritic enclaves, and **(E)** the basaltic rocks. Chondrite normalized rare Earth element diagrams of the **(B)** host quartz dioritic and dioritic rocks, **(D)** the dioritic host rocks, and **(F)** the basaltic rocks. Mid-ocean ridge basalt and chondrite normalizing values of Sun and McDonough (1989). Symbols of the Snoul pluton are the same as in Figure 7.

age from Late Ediacaran (~577 Ma) to Early Cretaceous (~118 Ma) whereas sample O05c has one early Triassic zircon (~240 Ma). The zircon ages of the diorites from this study are contemporaneous with Early Cretaceous granitic magmatism throughout the Dalat-Kratie Fold Belt of Vietnam and Cambodia (Nguyen et al., 2004a; Shellnutt et al., 2013; Breitfeld et al., 2020; Hennig-Breitfeld et al., 2021; Kasahara et al., 2021; Nong et al., 2021; Nong et al., 2022). Specifically, they correlate to a period of subduction-related (130–90 Ma) magmatism along the western margin of the Paleo-Pacific Ocean (Taylor and Hayes, 1983; Metcalfe, 2006; Yang, 2013; Hennig-Breitfeld et al., 2021; Waight et al., 2021).

Farther north along the SE coast of China, the Early Cretaceous period of arc-magmatism is referred to as the Late Yanshanian Orogen and is typified by I-type granite magmatism with subordinate S-type granite magmatism (Zhou et al., 2006; Li et al., 2012; Li et al., 2014; Dong et al., 2018; Shellnutt et al., 2020a; Suga and Yeh, 2020). From a geodynamic point of view, the Early Cretaceous Eurasian margin arc-magmatism is related to subduction of Paleo-Pacific oceanic crust (Maruyama et al., 1997; Yang, 2013; Wu et al., 2022).

Inherited zircons are more common in sample O20 whereas there was only one identified in O05c (~240 Ma). Sample O20 has the most inherited zircons (22) and a clear Paleozoic population (335–296 Ma) and one Late Ediacaran zircon (~577 Ma). There are eleven inherited zircons with a slightly older age range (112–118 Ma) than the weighted-mean ages of the diorite. We interpret these inherited zircons as being derived from an older period of spatially associated subduction-related magmatism as they have similar Hf isotopic values ($\varepsilon_{Hf}(t)$ = +13.2– +16.8) as the emplacement age zircons ($\varepsilon_{Hf}(t)$ = +12.1– +17.0). Moreover, the inherited Early Cretaceous (112–118 Ma) ages overlap with reported rock ages throughout the Dalat-Kratie Fold Belt of Vietnam and Cambodia (Nguyen et al., 2004a; Shellnutt et al., 2013; Hennig-Breitfeld et al., 2021; Kasahara et al., 2021; Nong et al., 2021). The Late Paleozoic (335–296 Ma) inherited zircons are contemporaneous with Middle Carboniferous

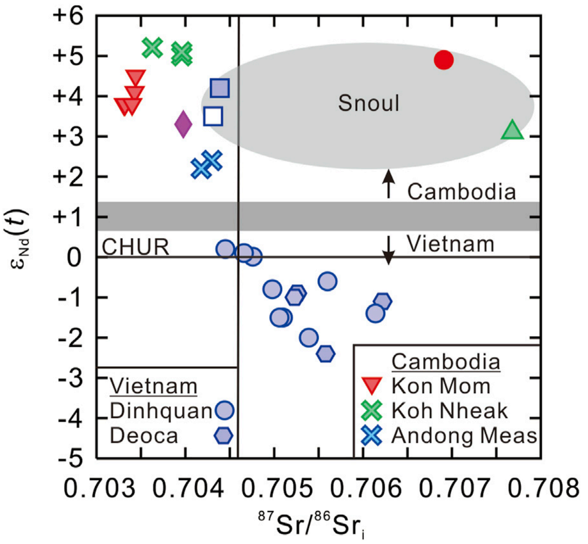

FIGURE 9
Sr-Nd isotopic data from the dioritic and quartz dioritic rocks of the Snoul pluton. Additional data from the Aptian-Albian volcanic-arc granites from southern Vietnam and eastern Cambodia (Nguyen et al., 2004a; Shellnutt et al., 2013; Cheng et al., 2019). Symbols of the Snoul pluton are the same as in Figure 7.

(336 ± 3 Ma) to Permian (267 ± 3 Ma) mafic and silicic rocks known throughout Indochina. The magmatic rocks may be related to an earlier period of subduction of the Paleotethys and back-arc extension prior to the amalgamation between the Sukhothai and Indochina terranes or subduction of the Paleo-Pacific plate (Hall and Sevastjanova, 2012; Burrett et al., 2014; 2021; Wang et al., 2018; Cheng et al., 2019; Kasahara et al., 2021; Shi et al., 2021; Waight et al., 2021; Breitfeld et al., 2022).

The Triassic zircon of O05c is contemporaneous with rocks in Cambodia as Cheng et al. (2019), Kasahara et al. (2021) and Waight et al. (2021) reported zircon U-Pb ages from 201.88 ± 0.36 Ma to 238.21 ± 0.31 Ma. The Triassic magmatism in Cambodia is interpreted to be related to subduction and back-arc extension associated with Paleotethys subduction along the western margin of the amalgamated Sukhothai-Indochina terranes (Sone and Metcalfe, 2008; Kasahara et al., 2021; Waight et al., 2021). Moreover, there is Triassic magmatism throughout Vietnam that may be related to subduction of the Paleo-Pacific plate (Hennig-Breitfeld et al., 2021).

Petrogenesis of the Snoul pluton, enclaves, and basaltic rocks

Tectonomagmatic discrimination of the quartz diorites, diorites, and basaltic rocks

The host rocks are geochemically (magnesian, metaluminous, calcic) similar to granitic rocks that are typical of the outboard portions of Cordilleran Batholiths or volcanic-arcs (Frost et al., 2001). Moreover, the rocks do not exceed CIPW normative corundum of 1% (Chappell and White, 2001) and their data fall within the fields of volcanic-arc or I-type granites in the tectonomagmatic discrimination diagrams of Pearce et al. (1984), Whalen et al. (1987), and Whalen and Hildebrand (2019) (Figure 10). The emplacement ages and location of the rocks are consistent with other volcanic-arc rocks in the eastern portion of the Dalat-Kratie belt of Vietnam and more broadly with the period of Late Yanshanian magmatism along the eastern margin of Eurasia (Nguyen et al., 2004a; Nguyen et al., 2004b; Shellnutt et al., 2013; Cheng et al., 2019; Hennig-Breitfeld et al., 2021; Kasahara et al., 2021).

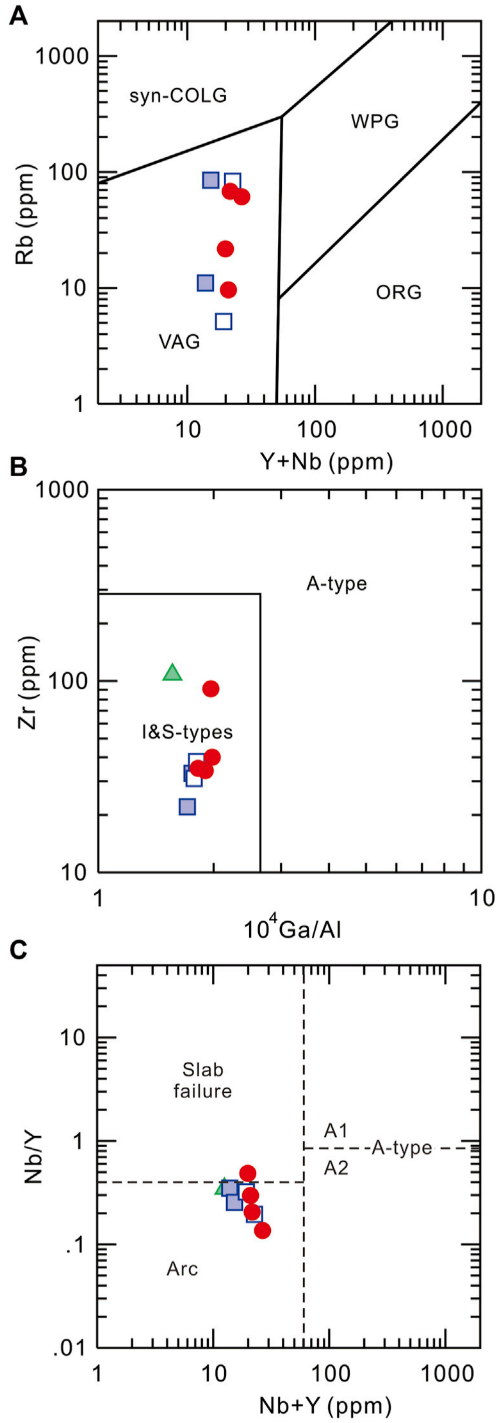

FIGURE 10
Tectonomagmatic discrimination of the dioritic and quartz dioritic rocks of the Snoul pluton of **(A)** Pearce et al. (1984), **(B)** Whalen et al. (1987), and **(C)** Whalen and Hildebrand (2019). Symbols of the Snoul pluton are the same as in Figure 7.

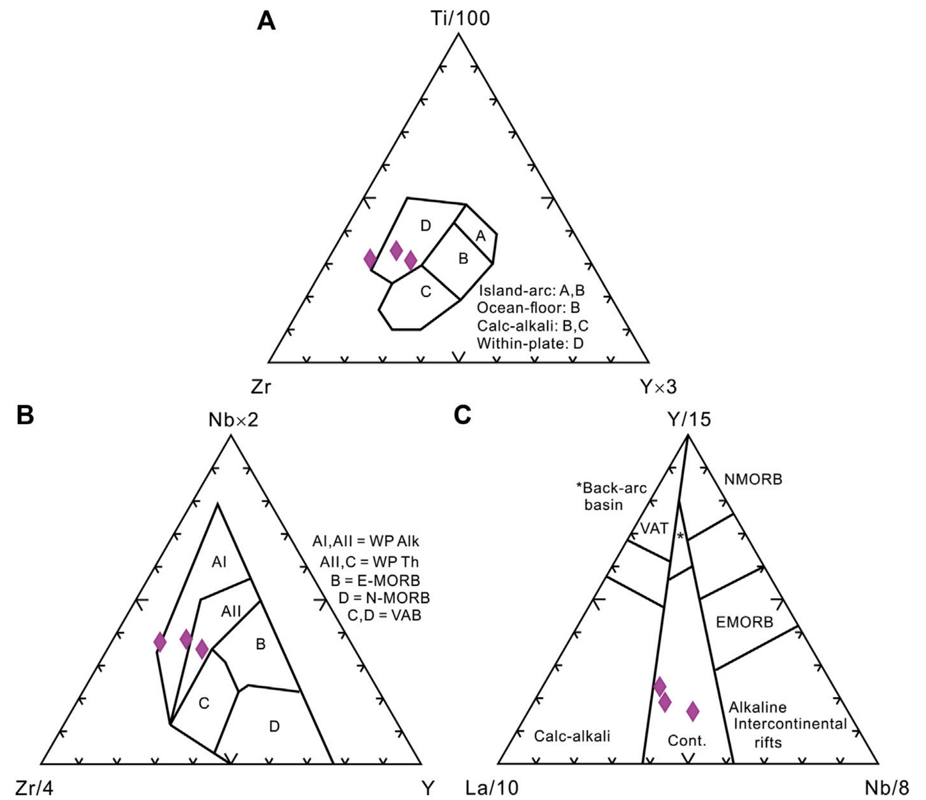

FIGURE 11
Tectonomagmatic discrimination of the basaltic rocks using the schemes of **(A)** Pearce and Cann (1973), **(B)** Meschede (1986), and **(C)** Cabanis and Lecolle (1989). WP Alk = within-plate alkaline basalt; WP Th = within-plate tholeiitic basalt; E-MORB = enriched mid-ocean ridge basalt; N-MORB = normal mid-ocean ridge basalt; VAB = volcanic-arc basalt; VAT = volcanic-arc tholeiite.

The dioritic (A17.4b, A17-7-en, A17-8-EN, A17.11b) enclaves (SiO_2 = 54–57 wt%) are chemically similar to the host diorites (A17-8-h, O05c, O20, O27a) as they are magnesian and metalumiunous, but tend to be calc-alkalic to calcic rather than calcic. The difference between calcic and calc-alkalic rocks, according to Frost et al. (2001), is that calc-alkalic rocks are representative of the main portions of Cordilleran Batholiths rather than the outboard portions. The subtle distinction between the enclaves and the host diorite may not be meaningful as it is likely that the two rock types are petrogenetically related whereby the enclaves are representative of the parental arc magmas of the quartz diorites. The petrogenetic relationship between the enclaves and host rock will be discussed later. Nevertheless, the enclaves fall within the volcanic-arc and I-type fields of Pearce et al. (1984), Whalen et al. (1987), and Whalen and Hildebrand (2019) and correspond to the ACG (amphibole-rich, calc-alkaline) granitoids of Barbarin (1999) (Figure 10).

The basaltic rocks are compositionally similar to transitional to mildly alkaline basalt (Figures 7A, 11). Petrographically, the rocks are not composed of cumulus minerals and their Eu/Eu* values (0.93–0.96) are close to unity. The Eu/Eu* values do not indicate significant fractionation or accumulation of plagioclase. In other words, the mafic rocks do not appear to be restites and the chilled margin texture is indicative of an intrusive contact rather than a xenolith. The application of three tectonomagmatic discrimination diagrams consistently show that the rocks plot as within-plate basalt typical of continental rift settings rather than convergent margin settings (Figure 11). The classification of the basaltic rocks as 'within-plate' is supportive of their intrusive nature (i.e., dyke) as they would be younger, but also likely correlative to the adjacent Neogene–Quaternary Phuoc Long flood basalt province (Nguyen and Flower, 1998; An et al., 2017).

Magma evolution of the silicic system

The quartz diorite and dioritic rocks are compositionally similar (magnesian, metaluminous) and show chemical evolution trends of major elements (decrease of TiO_2, Al_2O_3, Fe_2O_3t, MgO, CaO, Na_2O, and an increase of K_2O) against SiO_2 that may be indicative of magma compositional evolution. Moreover, the Sr-Nd isotopes of the host rocks ($^{87}Sr/^{86}Sr_i$ = 0.704389–0.707681; $\varepsilon_{Nd}(t)$ = +3.1– +4.9) are similar to the enclave ($^{87}Sr/^{86}Sr_i$ = 0.704313; $\varepsilon_{Nd}(t)$ = +3.5) and all rocks have similar chondrite normalized La/Yb (2.9–7.2) and Gd/Yb (1.1–1.6) ratios, low Nb/U (1.9–4.1), and high primitive mantle normalized Th/Nb (6.3–15.0) ratios. Consequently, it is possible that the diorites or enclave may be representative of the parental or earlier magma composition of the quartz diorites.

In order to evaluate the petrological relationship between the quartz diorites and the diorites we apply Rhyolite-MELTS (version 1.0.2) fractional crystallization modeling (Gualda et al., 2012). We select sample A17.11b (enclave) as the starting composition as it has the highest MgO content (~4.2 wt%), the second highest Ni (10 ppm) content, lowest Sr (282 ppm) content, and the second highest Mg# (52.7) of all the dioritic rocks. The starting conditions are not quantitatively constrained, however given that the rock is similar to

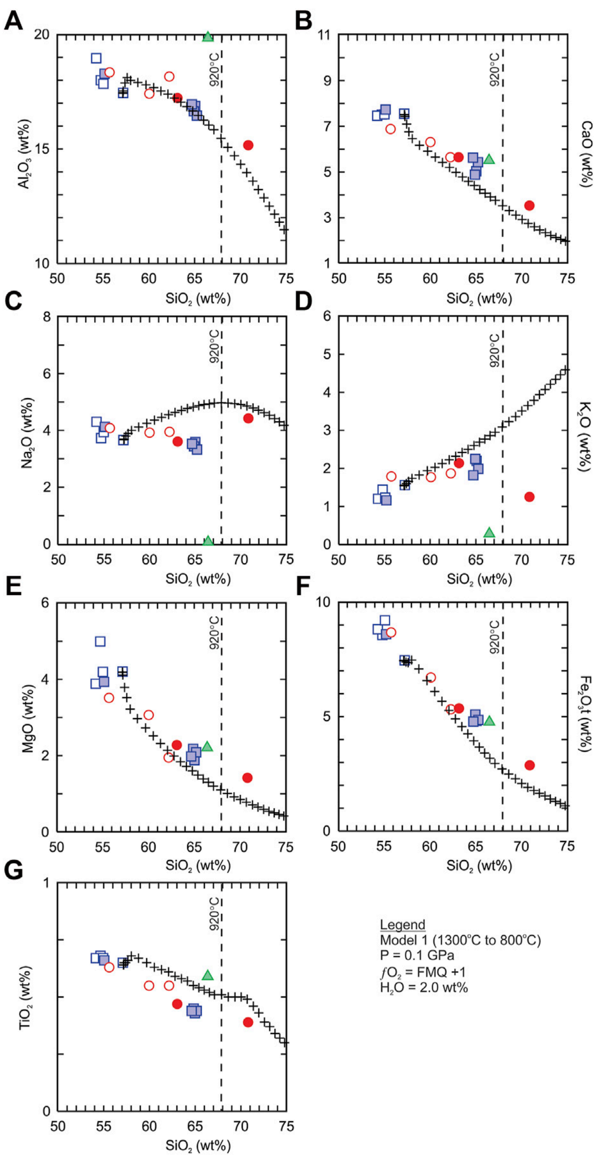

FIGURE 12
The results of hydrous fractional crystallization of the Snoul pluton at 0.1 GPa and fO_2 = ΔFMQ +1. **(A)** Al_2O_3 (wt%), **(B)** CaO (wt%), **(C)** Na_2O (wt%), **(D)** K_2O (wt%), **(E)** MgO (wt%), **(F)** Fe_2O_3t (wt%), and **(G)** TiO_2 (wt%) vs. SiO_2 (wt%). The residual silicic liquids compositions are at 10°C intervals. The complete modeling results are in online Supplementary Table S6. All data are normalized to 100%. Symbols of the Snoul pluton are the same as in Figure 7.

volcanic arc granite, we select conditions that are typical of convergent margin magma systems (Supplementary Table S6). The relative oxidation state is set to one log unit above the fayalite-magnetite-quartz buffer (ΔFMQ +1) as magnesian and calcic-calc alkalic rocks from arc settings tend to be associated with oxidizing conditions (Frost et al., 2001; Arculus, 2003). The initial water content was set to 2 wt% as most mafic arc magmas contain 2–6 wt% water content (Plank et al., 2013). The pressure of crystallization is set to 0.1 GPa (~3.7 km) which is indicative of the upper crust location of the pluton.

The residual liquid model curve is shown in Figure 12 with the complete results available in online Supplementary Supplementary Table S6. The liquid compositions are shown at 10°C intervals and the starting temperature was set to 1,300°C. The liquidus temperature is 1090°C when clinopyroxene ($Wo_{40}En_{47}Fs_{13}$) crystallizes. The compositional range of the silicic system is generated from ~1090°C to ~880°C. At 880°C, ~59% of the total magma system crystallized with ~41% liquid remaining. The fractionated assemblage from the liquidus temperature to 880°C is: clinopyroxene (1090°C–930°C), orthopyroxene (1070°C–880°C), plagioclase (1070°C–880°C), Fe-Ti (titanomagnetite) spinel (1050°C–910°C, 880 °C), and ilmenite (880 °C). The proportions, relative to the total solid, and compositional ranges of the fractionated minerals at 880°C are: clinopyoxene ($Wo_{40\text{-}30}En_{47\text{-}52}Fs_{13\text{-}18}$) = ~15.8%, orthopyroxene = 13.6%, plagioclase ($An_{74\text{-}36}$) = 61.9%, spinel (titanomagnetite) = 8.6%, and ilmenite = 0.02%.

The compositional variability of the rocks can be explained primarily by crystal fractionation (~90%) of clinopyroxene, orthopyroxene, and plagioclase, although Na_2O tends to be ~1 wt% higher for rocks with 63–67 wt% SiO_2 until matching the high SiO_2 sample (Figure 12). The fractionating mineral assemblage is consistent with the decrease in Sc, Ni, Co, and Sr concentration with increasing SiO_2 content of the rocks. However, two quartz diorites (A17.1ah and A17.3b) have Eu/Eu* values greater than one suggesting that Eu may have increased in the magma system before the onset of feldspar fraction or that the rocks are composed of cumulus plagioclase. Alternatively, the higher Eu/Eu* values could be related to a high magmatic oxidation state as this would favour Eu^{3+} which does not partition as readily into feldspar as Eu^{2+} (Cicconi et al., 2022). Nevertheless, the model shows good agreement from the intermediate rocks to the diorites indicating that they may represent a cogenetic magma that developed in the upper crust under hydrous and oxidizing conditions. We cannot eliminate the possibility that crustal contamination or other syn/post-emplacement processes affected the system as inherited zircons were identified, but only that crystal fractionation was the primary process of magma differentiation.

Magma source

The fractional crystallization modeling and Sr-Nd isotopes are supportive of a cogenetic origin of the diorites and quartz diorites of the Snoul pluton. Moreover, it is likely that the diorites are similar to the original parental magma. The Sr-Nd-Hf isotopes ($^{87}Sr/^{86}Sr_i$ = 0.704313 and 0.706909; $\varepsilon_{Nd}(t)$ = +3.5 and +4.9; $\varepsilon_{Hf}(t)$ = +7.0– +17.0) of the diorites rocks are moderately depleted and indicative of either a juvenile crustal source or a depleted mantle source that was enriched by subduction-related or crustal materials (i.e., melt and/or fluids). That is, the parental magma may have been derived by partial melting of juvenile mafic crust (Defant and Drummond, 1990; Rapp and Watson, 1995; Rapp et al., 1999; Moyen, 2009; Castillo, 2012), by partial melting of a pyroxenitic mantle source (Kogiso et al., 2004; Straub et al., 2008; Straub et al., 2011), or was derived by mixing between a basaltic magma and a crustal melt.

We do not think that the parental magma of the dioritic rocks (SiO_2 = 54–61 wt%) was derived by mixing between a basaltic magma and crustal magma as the Eu/Eu* values are 0.97–0.98 and the Ni concentration is ≤12 ppm. It is unlikely that mixing between an isotopically enriched upper crustal melt with a primitive arc basalt could yield a hybrid composition that has such a high Eu/Eu* value and low Ni concentration. Furthermore, average middle and lower crust compositions of Rudnick and Gao (2014) have relatively high Ni content (33–88 ppm) and high Eu/Eu* values (>0.95) and thus any melt composition derived from either would be insufficient to drive Ni contents lower than 12 ppm while increasing the SiO_2 content by 3–5 wt% and maintaining an $\varepsilon_{Nd}(t)$ values greater than +3. Therefore, it is likely that the dioritic rocks are either derived by melting of a pyroxenitic mantle source or partial melting of a subducted oceanic slab or juvenile lower crust.

Silicic magma (SiO_2 = 55–65 wt%) may be generated by direct melting of 'reaction pyroxenite' peridotite (Straub et al., 2008; Straub et al., 2011). However, these magmas tend to have high Mg# (>55) and Ni > 50 ppm as they inherit the high MgO and FeO ratio of the original peridotite mantle (Baker et al., 1994; Straub et al., 2011). The melts also tend to have TiO_2 > 0.7 wt% (Kogiso et al., 2004). The dioritic rocks have Ni ≤ 12 ppm, Mg# of 42.1–53.6, and TiO_2 < 0.7 wt%. In comparison, adakitic melts generated by melting of subducted slab tend to have SiO_2 ≥ 56 wt%, Al_2O_3 ≥ 15 wt%, MgO <3 wt% (rarely >6 wt%), Sr ≥ 400 ppm, Y ≤ 18 ppm, Yb ≤ 1.9 ppm, Sr/Y > 40, and Ni < 50 ppm (Defant and Drummond, 1990; Castillo, 2012). The diorites of this study, in particular samples O20 and O27a, are somewhat similar to adakitic rocks as they have SiO_2 = 54.8–61.8 wt%, Al_2O_3 > 17.5 wt%, MgO ≤5 wt%, Sr = 282–679 ppm, Y = 14.6–23.5 ppm, Yb = 1.65–2.20 ppm, and Sr/Y = 18.5–41.9, but they do not fit perfectly within the low-SiO_2 or high-SiO_2 adakite groupings of Martin et al. (2005). The moderately depleted isotopic compositions and Late Neoproterozoic to Paleozoic Nd and Hf depleted mantle model ages imply the rocks are derived from juvenile crust whereas their negative primitive mantle normalized anomalies of Nb are consistent with continental crust generated at an arc setting. Although we cannot be more certain on the exact nature of the source for the parental magmas, we conclude that it is either mafic, juvenile, arc-related lower crust of the Indochina terrane or the upper subducted Paleo-Pacific oceanic crust. If the former is true, then it offers an explanation for the distinct change in the source composition of the contemporaneous Aptian-Albian volcanic-arc rocks across the Dalat zone as granitic rocks to the east are isotopic different ($^{87}Sr/^{86}Sr_i$ = 0.70444–0.71188; $\varepsilon_{Nd}(t)$ = −2.4- +0.2) (Figure 9).

Magma evolution of the mafic system

The origin of the basaltic rocks is likely different from the silicic system as they are compositionally similar to within-plate basalt rather than arc basalt. The basaltic rocks have similar primitive mantle normalized and chondrite normalized incompatible elemental patterns suggesting that they are petrogenetically related. Specifically, the rocks have modest negative Nb anomalies and very similar light rare Earth element enriched patterns (Figures 8E, F). The compositions are not primary as their Mg# (50.1–61.7) and MgO (4.88–9.11 wt%) and Ni (24–205) contents are evolved. Sample A17.10b is the most primitive, but the CaO (9.40–10.65 wt%) contents are low and Fe_2O_3t (9.57–11.21 wt%) contents are high. The low Mg# and CaO and absence of negative Eu/Eu* (0.93–0.96) indicates that the rocks underwent fractionation of mafic silicate minerals (e.g., olivine, clinopyroxene) with minimal plagioclase fractionation.

The results of fractional crystallization modeling using Rhyolite-MELTS and a starting composition similar to sample A17.10b with a pressure of 0.1 GPa, initial water content of 1.25 wt%, and fO_2 at the Ni-NiO (ΔFMQ +0.7) buffer is shown in Figure 13 (Supplementary Table S6). The results indicate that fractionation of olivine (8.2 vol%), clinopyroxene (12.8 vol%), plagioclase (2.2 vol%), and spinel (0.85 vol %) from 1,260–1,090°C with ~75.1 vol% liquid remaining can explain the chemical variability of the basaltic rocks (Figure 13). Moreover, the high La/Yb_N (11.2–13.2) and Tb/Yb_{PM} (1.9–2.2) ratios indicate that the mantle source was garnet bearing and had a minimum depth of melting of 60–70 km which is similar to estimates for the Neogene–Quaternary flood basalts of Southeast Asia (Nguyen and Flower, 1998; Wang et al., 2002).

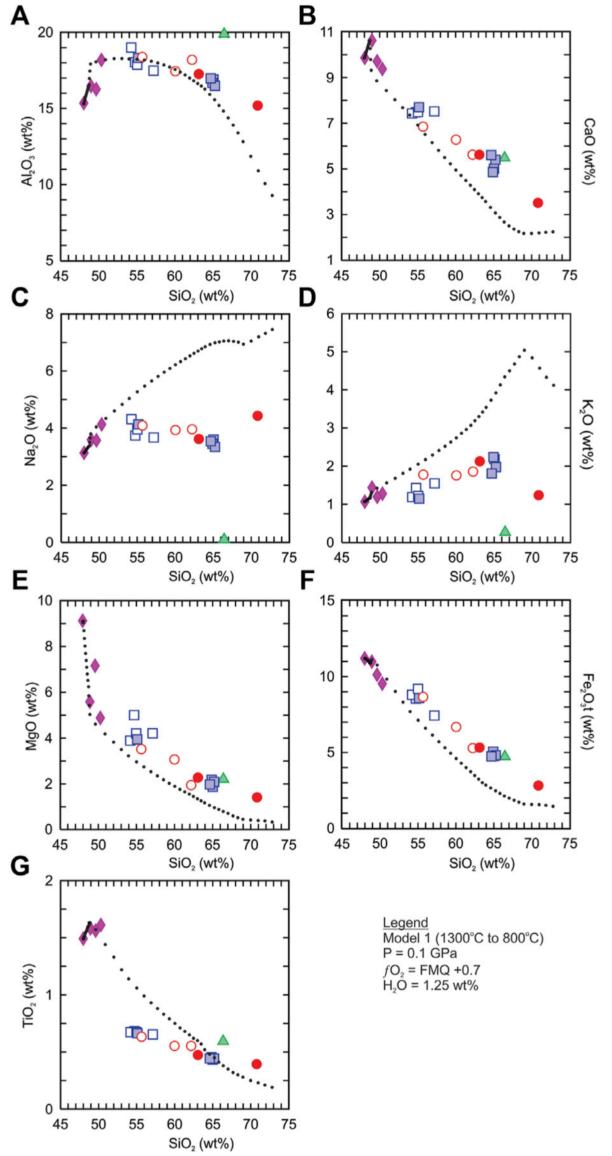

FIGURE 13
The results of hydrous fractional crystallization of the basaltic rocks from the Snoul pluton at 0.1 GPa and fO_2 = ΔFMQ +0.7. **(A)** Al_2O_3 (wt%), **(B)** CaO (wt%), **(C)** Na_2O (wt%), **(D)** K_2O (wt%), **(E)** MgO (wt%), **(F)** Fe_2O_3t (wt%), and **(G)** TiO_2 (wt%) vs. SiO_2 (wt%). The residual silicic liquids compositions are at 10°C intervals. The complete modeling results are in online Supplementary Table S6. All data are normalized to 100%. Symbols of the Snoul pluton are the same as in Figure 7.

The most extensive eruption of within-plate alkaline basalt across SE Asia occurred during the Late Cenozoic (<10 Ma) with correlative rocks identified in eastern Cambodia (Flower et al., 1993; Nguyen and Flower, 1998; Fedorov and Koloskov, 2005; An et al., 2017; Zhao et al., 2021). If we assume an emplacement age of 10 Ma for the basaltic

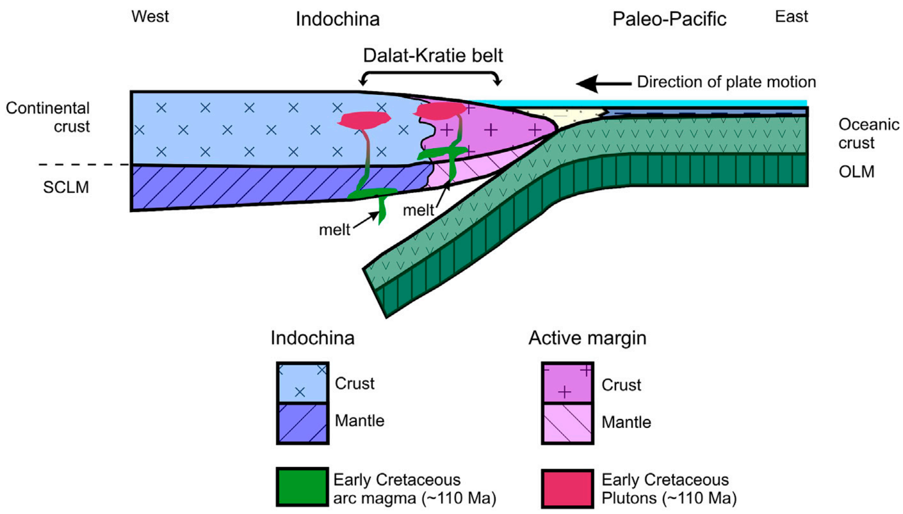

FIGURE 14
Conceptual model for the genesis of the Cretaceous (130-90 Ma) volcanic-arc granites of the Dalat-Kratie belt. Subduction of the Paleo-Pacific plate beneath the Indochina terrane belt generates arc magmas that may be derived from the subducted slab, lower crust, or from mixed crustal/mantle sources. The granitic plutons closer (purple region) to arc front are more likely to be isotopically enriched whereas those located farther (blue region) from the arc front are more likely to be isotopically juvenile. It is possible that the isotopic differences are an intrinsic feature of the Indochina terrane and that there may exist a domain boundary within the southeast Indochina terrane.

rocks of this study then the initial Sr-Nd ratios ($^{87}Sr/^{86}Sr_i$ = 0.703978; $\varepsilon_{Nd}(t)$ = +4.2) are indicative of a moderately depleted source. It is likely that the basaltic rocks of this study were emplaced during a period of regional tensional plate stress and that their source (i.e., garnet-spinel bearing peridotite) may be indicative of the lithospheric mantle in this part of the Indochina terrane.

Migration of the continental-arc or discovery of a terrane boundary?

Many continental and island arcs show evidence of magmatic migration over time (e.g., Lesser Antilles, Andes, Sunda) that is thought to be related to changes in the subducting plate dynamics (Kay et al., 2005; He and Xu, 2012; Allen et al., 2019; Lai et al., 2021). The Late Mesozoic granites of eastern China are an example of secular variation of granitic batholiths in a convergent margin regime as magmatism changed from one of sinistral strike-slip compression during the Jurassic to an active continental margin during the Early Cretaceous (Zhou et al., 2006; Dong et al., 2018). The Cretaceous granitic batholiths of eastern China show chemo-temporal transition from subduction-related Cordilleran-type batholiths during the Early Cretaceous (130–100 Ma) to extension-related A-type granitic batholiths during the Late Cretaceous (<90 Ma) (Zhou and Li, 2000; Zhou et al., 2006; Li et al., 2012). Correlative with the Late Yanshanian granites of eastern China are the Early Cretaceous granitic batholiths of the southern Indochina terrane (Nguyen et al., 2004a; Nguyen et al., 2004b; Shellnutt et al., 2013).

The reported ages of the Dalat-Kratie granites are mostly between ~120 Ma and ~80 Ma and show a chemical transition from Cordilleran I-type granites to post-collisional (A-type) granites over time (Nguyen et al., 2004a; Nguyen et al., 2004b; Shellnutt et al., 2013; Hennig-Breitfeld et al., 2021). Although there is a compositional transition from I-type granite to A-type granite, there does not appear to be a spatial correlation as the older I-type granites (120-115) geographically overlap with the younger I-type granites (110-90 Ma) and the A-type granites (<90 Ma) (Nguyen et al., 2004a; Nguyen et al., 2004b; Shellnutt et al., 2013; Cheng et al., 2019; Kasahara et al., 2021; Hennig-Breitfeld et al., 2021; Waight et al., 2021; Nong et al., 2022). However, there is a distinct change in the Sr-Nd isotopic compositions of the I-type granites in Cambodia compared to the granites of similar age in Vietnam (Figure 9).

The precise reason for the isotopic change is not clear, but it must be related to the parental magma source. Consequently, there are two possibilities: 1) there is a change in the lithospheric composition of each region, or 2) there were differences in the amount of isotopically enriched components in the genesis of the parental magmas. If the parental magmas of the I-type granites of each region are derived primarily by lithospheric melting then the western region must be isotopically juvenile compared to the eastern region. This could imply that there is a heretofore unseen lithotectonic boundary between the two regions (c.f., Dijkstra and Hatch, 2018). Alternatively, it could reflect differences in the amount of enriched material (e.g., fluids, melts) originating either from subducted sediment or crustal melts that is incorporated into the parental magmas whether they are derived from the mantle or subducted slab. That is, there was more enriched material involved in the genesis of the granitoids from Vietnam than the granitoids from Cambodia.

We cannot be certain which of the two scenarios is more likely, although we tend to favour the possibility that there is a domain boundary between eastern Cambodia and southern Vietnam (Figure 14). The western region of the Dalat-Kratie belt in Vietnam and Cambodia is referred to as the Srepok-Tay Nam Bo orogenic belt (c.f., Hennig-Brietfeld et al., 2021). Consequently, it is possible that the Srepok-Tay Nam Bo orogenic belt and the Dalat-Kratie belt are compositionally and tectonically distinct regions of the Indochina terrane. Our preferred interpretation is based on the fact that the Carboniferous-Permian (343–253 Ma) inherited zircons from the Late Cretaceous (86.6 ± 1.6 Ma) Ankroet "A-type" granite of Vietnam have negative $\varepsilon_{Hf}(t)$ values (−10.2– −3.3; Shellnutt et al., 2013) whereas the Carboniferous-Permian (335–296 Ma) inherited zircons from the Snoul pluton have positive $\varepsilon_{Hf}(t)$ values (+3.9– +15.5). Furthermore, the single Triassic (249 ± 5 Ma, 1σ) inherited zircon from Ankroet has a highly negative $\varepsilon_{Hf}(t)$ value (−17.2) whereas in the Snoul pluton the Early Triassic (240 Ma) inherited zircon has near chondritic value $\varepsilon_{Hf}(t)$ values (+1.2). Thus, the Hf isotopes of the inherited Paleozoic zircons and the whole rock Sr-Nd isotopes indicate that the isotopic differences between the two regions are likely to be an intrinsic feature of the Indochina lithosphere that predates the Cretaceous (e.g., Shellnutt et al., 2020b). Therefore, it possible that the lithosphere of the southern Indochina terrane is composed of distinct lithotectonic domains.

Conclusion

The quartz diorites and diorites of the Snoul pluton are compositionally similar to volcanic-arc granitoids. The rocks were emplaced during the Early Cretaceous (107.5 ± 0.3 Ma, 109.2 ± 0.4 Ma) subduction of the Paleo-Pacific plate beneath the Indochina terrane. The whole rock Sr-Nd isotopes show that the host rocks ($^{87}Sr/^{86}Sr_i$ = 0.704389–0.707681; $\varepsilon_{Nd}(t)$ = +3.1– +4.9) are similar to the enclave ($^{87}Sr/^{86}Sr_i$ = 0.704313; $\varepsilon_{Nd}(t)$ = +3.5) and indicate that they are part of the same magmatic system.

Fractional crystallization modeling under oxidizing (ΔFMQ +1), hydrous (H_2O = 2 wt%), and low pressure (p = 0.1 GPa) conditions shows that it is possible that the dioritic rocks are representative of the parental magma composition of the system. Moreover, some of the diorites are compositionally similar to adakitic rocks which may suggest that they were originally derived by partial melting of juvenile mafic crust of the Indochina terrane. If this is true, then it may explain the isotopic change in granitic rocks from enriched Sr-Nd values in Vietnam to moderately depleted values in Cambodia.

The basaltic rocks represent a different magmatic system as they are compositionally similar to within-plate basalt rather than volcanic-arc basalt. Fractional crystallization modeling using the most primitive basalt as the parental composition can explain the chemical variability within the basaltic rocks. The Sr-Nd isotopic values are moderately depleted and are similar to host intrusion. We think that it is likely that the basaltic rocks are contemporaneous with the Neogene–Quaternary flood basalts of SE Asia and petrogenetically unrelated to the Snoul pluton.

Data availability statement

The original contributions presented in the study are included in the article/Supplementary Material, further inquiries can be directed to the corresponding author.

Author contributions

GM and JC conceived of the study and collected the samples. JS, GM, and JW wrote the manuscript. JW measured the zircon U-Pb and Hf isotopes, K-LW assisted with the whole rock Sr-Nd isotopes and whole rock trace elements, and JS measured the whole rock major elements. All authors contributed to the manuscript, read, and approved the submitted version.

Funding

This project received support from the National Science and Technology Council (Taiwan) through grant 111-2116-M-003-006.

Acknowledgments

We thank Fu-Lung Wang and Robert Hsieh for their help during sample preparation and analytical work and Southern Gold (Cambodia) for sample provision.

Conflict of interest

The authors declare that the research was conducted in the absence of any commercial or financial relationships that could be construed as a potential conflict of interest.

Publisher's note

Supplementary material

The Supplementary Material for this article can be found online at: https://www.frontiersin.org/articles/10.3389/feart.2023.1110568/full#supplementary-material

References

Allen, R. W., Collier, J. S., Stewart, A. G., Henstock, T., Goes, S., Rietbrock, A., et al. (2019). The role of arc migration in the development of the esser Antilles: new tectonic model for the enozoic evolution of the eastern aribbean. *Geology* 47, 891–895. doi:10.1130/G46708.1

An, A.-R., Choi, S. H., Yu, Y., and Lee, D.-C. (2017). Petrogenesis of ate enozoic basaltic rocks from southern Vietnam. *Lithos* 272-273, 192–204. doi:10.1016/j.lithos.2016.12.008

Arculus, R. J. (2003). Use and abuse of the terms calcalkaline and calcalkalic. *J. Petrol* 44, 929–935. doi:10.1093/petrology/44.5.929

Baker, M. B., Grove, T. L., and Price, R. (1994). Primitive basalts and andesites from the Mt. Shasta region, N. California: roducts of varying melt fraction and water content. *Contrib. Mineral. Petrol.* 118, 111–129. doi:10.1007/BF01052863

Barbarin, B. (1999). A review of the relationships between granitoid types, their origins and their geodynamic environments. *Lithos* 46, 605–626. doi:10.1016/S0024-4937(98)00085-1

Blichert-Toft, J., and Albarede, F. (1997). The Lu-Hf isotope geochemistry of chondrites and the evolution of the mantle-crust system. *Earth Planet. Sci. Lett.* 148, 243–258. doi:10.1016/S0012-821X(97)00040-X

Bouilhol, P., Jagoutz, O., Hanchar, J. M., and Dudas, F. O. (2013). Dating the India-Eurasia collision through arc magmatic records. *Earth Planet. Sci. Lett.* 366, 163–175. doi:10.1016/j.epsl.2013.01.023

Breitfeld, H. T., Davies, L., Hall, R., Armstrong, R., Forster, M., Lister, G., et al. (2020). Mesozoic aleo-acific subduction beneath SW orneo: U-Pb geochronology of the chwaner granitoids and the inoh metamorphic group. *Front. Earth Sci.* 8, 568715. doi:10.3389/feart.2020.568715

Breitfeld, H. T., Hennig-Breitfeld, J., Boudagher-Fadel, M., Schmidt, W. J., Meyer, K., Reinprecht, J., et al. (2022). Provenance of Oligocene-Miocene sedimentary rocks in the Cuu Long and Nam Con Son basins, Vietnam and early history of the Mekong River. *Int. J. Earth Sci* 111, 1773–1804.

Burrett, C., Udchachon, M., and Thassanapak, H. (2021). The Truong Son, oei-hetchabun, and Kontum erranes in Indochina: rovenance, rifting, and collisions. *Front. Earth Sci.* 9, 603565. doi:10.3389/feart.2021.603565

Burrett, C., Zaw, K., Meffre, S., Lai, C. K., Khositanont, S., Chaodumrong, P., et al. (2014). The configuration of reater Gondwana–Evidence from LA ICPMS, U–Pb geochronology of detrital zircons from the alaeozoic and esozoic of Southeast Asia and China. *Gondwana Res* 26, 31–51. doi:10.1016/j.gr.2013.05.020

Cabanis, B., and Lecolle, M. (1989). Le diagramme La/10–Y/15–Nb/8: n outil pour la discrimination des series volcanique et la mise en evidence des processus de melange et/ou de contamination crustale. *Acad. Sci. Ser. II* 309, 2023–2029.

Carter, A., and Clift, P. D. (2008). Was the Indosinia orogeny a Triassic mountain building or a thermotectonic reactivation event? *C. R. Geosci.* 340, 83–93. doi:10.1016/j.crte.2007.08.011

Carter, A., Roques, D., Bristow, C., and Kinny, P. (2001). Understanding esozoic accretion in outheast Asia: ignificance of riassic thermotectonism (ndosinian orogeny) in Vietnam. *Geology* 29, 211–214. doi:10.1130/0091-7613(2001)029<0211:UMAISA>2.0.CO;2

Castillo, P. R. (2012). Adakite petrogenesis. *Lithos* 134-135, 304–316. doi:10.1016/j.lithos.2011.09.013

Chappell, B. W., and White, J. R. (2001). Two contrasting granite types: 25 years later. *Aust. J. Earth Sci.* 48, 489–499. doi:10.1046/j.1440-0952.2001.00882.x

Chauvel, C., Lewin, E., Carpentier, M., Arndt, N. T., and Marini, J.-C. (2008). Role of recycled oceanic basalt and sediment in generating the Hf-Nd mantle array. *Nat. Geosci.* 1, 64–67. doi:10.1038/ngeo.2007.51

Cheng, R., Uchida, E., Katayose, M., Yarimizu, K., Shin, K.-C., Kong, S., et al. (2019). Petrogenesis and tectonic setting of ate aleozoic to ate esozoic igneous rocks in Cambodia. *J. Asian Earth Sci.* 185, 104046. doi:10.1016/j.jseaes.2019.104046

Chu, N. C., Taylor, R. N., Chavagnac, V., Nesbitt, R. W., Boella, R. M., Milton, J. A., et al. (2002). Hf isotope ratio analysis using multi-collector inductively coupled plasma mass spectrometry: n evaluation of isobaric interference corrections. *J. Anal. At. Spect.* 17, 1567–1574. doi:10.1039/B206707B

Cicconi, M. R., Le Losq, C., Henderson, G. S., and Neuville, D. R. (2021). "The redox behaviour of rare elements," in *Magma edox eochemistry*. Editors R. Moretti and D. R. Neuville (New York, USA: American Geophysical Union Geophysical Monograph), 381–398.

Corfu, F., Hanchar, J. M., Hoskin, P. W. O., and Kinny, P. (2003). Atlas of zircon textures. *Rev. Mineral. Geochem.* 53, 469–500. doi:10.2113/0530469

Cox, K. G., Bell, J. D., and Pankhurst, R. J. (1979). *The interpretation of igneous rocks*. London, UK: George Allen and Unwin Ltd, 450.

Defant, M. J., and Drummond, M. S. (1990). Derivation of some modern arc magmas by melting of young subducted lithosphere. *Nature* 347, 662–665. doi:10.1038/347662a0

Dijkstra, A., and Hatch, C. (2018). Mapping a hidden terrane boundary in the mantle lithosphere with lamprophyres. *Nat. Comm.* 9, 3770. doi:10.1038/s41467-018-06253-7

Dong, S., Zhang, Y., Li, H., Shi, W., Xue, H., Li, J., et al. (2018). The anshan orogeny and late esozoic multi-plate convergence in ast-Asia–Commemorating 90th years of the "Yanshan Orogeny". *Sci. China Earth Sci.* 61, 1888–1909. doi:10.1007/s11430-017-9297-y

Faure, M., Lin, W., Monié, P., and Meffre, S. (2008). Palaeozoic collision between the North and South China blocks, Triassic intracontinental tectonics, and the problem of the ultrahigh-pressure metamorphism. *C. R. Geosci.* 340, 139–150. doi:10.1016/j.crte.2007.10.007

Faure, M., Nguyen, V. V., Hoai, L. T. T., and Lepvrier, C. (2018). Early aleozoic or arly-iddle riassic collision between the South China and Indochina locks: he controversy resolved? Structural insights from the on um massif (entral Vietnam). *J. Asian Earth Sci.* 166, 162–180. doi:10.1016/j.jseaes.2018.07.015

Fedorov, P. I., and Koloskov, A. V. (2005). Cenozoic volcanism of southeast Asia. *Petrology* 13, 352–380. doi:10.1038/s41598-018-20712-7

Flower, M. F. J., Nguyen, H., Nguyen, T. Y., Nguyen, X. B., McCabe, R. J., and Harder, S. H. (1993). Cenozoic magmatism in Indochina: ithosphere extension and mantle potential temperature. *Geol. Soc. Malays Bull.* 33, 211–222. doi:10.7186/bgsm33199316

Frost, B. R., Barnes, C. G., Collins, W. J., Arculus, R. J., Ellis, D. J., and Frost, C. D. (2001). A geochemical classification for granitic rocks. *J. Petrol.* 42, 2033–2048. doi:10.1093/petrology/42.11.2033

Griffin, W. L., Belousova, E. A., Shee, S. R., Pearson, N. J., and O'Reilly, S. Y. (2004). Archean crustal evolution in the northern ilgarn raton: U–Pb and Hf-isotope evidence from detrital zircons. *Precambrian Res.* 131, 231–282. doi:10.1016/j.precamres.2003.12.011

Griffin, W. L., Pearson, N. J., Belousova, E., Jackson, S. E., van Achterbergh, E., O'Reilly, S. Y., et al. (2000). The Hf isotope composition of cratonic mantle: LAM-MC-ICPMS analysis of zircon megacrysts in kimberlites. *Geochim. Cosmochim. Ac.* 64, 133–147. doi:10.1016/S0016-7037(99)00343-9

Gualda, G. A. R., Ghiorso, M. S., Lemons, R. V., and Carley, T. L. (2012). Rhyolite-MELTS: modified calibration of MELTS optimized for silica-rich, fluid-bearing magmatic systems. *J. Petrol.* 53, 875–890. doi:10.1093/petrology/egr080

Hall, R. (2012). Late urassic-enozoic reconstructions of the Indonesian region and the Indian cean. *Tectonophysics* 570-570, 1–41. doi:10.1016/j.tecto.2012.04.021

Hall, R., and Sevastjanova, I. (2012). Australian crust in Indonesia. *Aust. J. Earth Sci.* 59, 827–844. doi:10.1080/08120099.2012.692335

Hall, R. (2017). Southeast Asia: ew views of the geology of the Malay rchipelago. *Annu. Rev. Earth Planet. Sci.* 45, 331–358. doi:10.1146/annurev-earth-063016-020633

He, Z.-Y., and Xu, X.-S. (2012). Petrogenesis of the ate anshanian mantle-derived intrusions in southeastern China: esponse to the geodynamics of aleo-Pacific plate subduction. *Chem. Geol.* 328, 208–221. doi:10.1080/08120099.2012.692335

Hennig-Breitfeld, J., Breitfeld, H. T., Sang, D. Q., Vinh, M. K., Long, T. V., Thirlwall, M., et al. (2021). Ages and character of igneous rocks of the Da Lat zone in SE Vietnam and adjacent offshore regions (Cuu long and Nam Con Son basins). *J. Asian Earth Sci.* 218, 104878. doi:10.1016/j.jseaes.2021.104878

Hutchinson, C. S. (2014). Tectonic evolution of southeast Asia. *Bull. Geol. Soc. Malays* 60, 1–18. doi:10.1016/j.jseaes.2021.104878

Jackson, S. E., Pearson, N. J., Griffin, W. L., and Belousova, E. A. (2004). The application of laser ablation-inductively coupled plasma-mass spectrometry to *in situ* U–Pb zircon geochronology. *Chem. Geol.* 211, 47–69. doi:10.1016/j.chemgeo.2004.06.017

Jiang, H., Li, W.-Q., Zhao, K.-D., Zhang, D., and Jiang, S.-Y. (2021). Middle riassic diorites from the Loei Fold Belt, NE Thailand: etrogenesis and tectonic implications in the context of aleotethyan subduction. *Lithos* 382-383, 105955. doi:10.1016/j.lithos.2020.105955

Kasahara, N., Niki, S., Uchida, E., Yarimizu, K., and Cheng, R. (2021). Zircon U-Pb chronology on plutonic rocks from northeastern Cambodia. *Heliyon* 7, e06752. doi:10.1016/j.heliyon.2021.e06752

Kay, S. M., Godoy, E., and Kurtz, A. (2005). Episodic arc migration, crustal thickening, subduction erosion, and magmatism in the south-central Andes. *Geol. Soc. Am. Bull.* 117, 67–88. doi:10.1130/B25431.1

Kogiso, T., Hirschmann, M. M., and Pertermann, M. (2004). High-pressure partial melting of mafic lithologies in the mantle. *J. Petrol.* 45, 2407–2422. doi:10.1093/petrology/egh057

Lai, Y.-M., Chung, S.-L., Ghani, A. A., Murtadha, S., Lee, H.-Y., and Chu, M.-F. (2021). Mid-Miocene volcanic migration in the westernmost Sunda arc induced by India-Eurasia collision. *Geology* 49, 713–717. doi:10.1130/G48568.1

Lan, C.-Y., Chung, S.-L., Long, T. V., Lo, C.-H., Lee, T.-Y., Mertzman, S. A., et al. (2003). Geochemical and Sr-Nd isotopic constraints from the Kontum massif, central Vietnam on the crustal evolution of the Indochina block. *Precambrian Res.* 122, 7–27. doi:10.1016/S0301-9268(02)00205-X

Lepvrier, C., Maluski, H., Tich, V. V., Leyreloup, A., Thi, P. T., and Vuong, N. V. (2004). The arly riassic ndosinian orogeny in Vietnam (Truong Son elt and Kontum assif); implications for the geodynamic evolution of Indochina. *Tectonophysics* 393, 87–118. doi:10.1016/j.tecto.2004.07.030

Lepvrier, C., Nguyen, V. V., Maluski, H., Phan, T. T., and Tich, V. V. (2008). Indosinian tectonics in Vietnam. *C. R. Geosci.* 340, 94–111. doi:10.1016/j.crte.2007.10.005

Li, Z.-X., Li, X.-H., Chung, S.-L., Lo, C.-H., Xu, X., and Li, W.-X. (2012). Magmatic switch-on and switch-off along the South China continental margin since the ermian: ransition from an ndean-type to a estern acific-type plate boundary. *Tectonophysics* 532-535, 271–290. doi:10.1016/j.tecto.2012.02.011

Li, Z.-X., and Li, X.-H. (2007). Formation of the 1300-km-wide intracontinental orogeny and post-orogenic magmatic province in esozoic outh China: flat-slab subduction model. *Geology* 35, 179–182. doi:10.1130/G23193A.1

Li, Z., Qiu, J.-S., and Yang, X.-M. (2014). A review of the geochronology and geochemistry of ate anshanian (retaceous) plutons along the ujian coastal area of southeastern China: mplications for magma evolution related to slab break-off and rollback in the retaceous. *Earth-Sci. Rev.* 128, 232–248. doi:10.1016/j.earscirev.2013.09.007

Liu, Y. S., Gao, S., Hu, Z. C., Gao, C. G., Zong, K. Q., and Wang, D. B. (2010). Continental and oceanic crust recycling-induced melt-peridotite interactions in the rans-orth China rogen: U-Pb dating, Hf isotopes and trace elements in zircons from mantle xenoliths. *J. Petrol.* 51, 537–571. doi:10.1093/petrology/egp082

Ludwig, K. R. (2008). *Isoplot 3.6; A eochronology oolkit for icrosoft xcel*. Berkeiey, CA, USA: Berkeley Geochronology Center, 77.

Machado, N., and Simonetti, A. (2001). "U–Pb dating and Hf isotopic composition of zircons by laser ablation-MC-ICP-MSA,". Editor P. Sylvester, 29, 121–146. *Laser Earth Sci Princ Appl Course Assoc. Canada.* doi:10.1016/j.rgg.2016.01.013

Martin, H., Smithies, R. H., Rapp, R., Moyen, J.-F., and Champion, D. (2005). An overview of adakite, tonalite-trondhjemite-quartz diorite (TTG), and sanukitoid: elationships and some implications for crustal evolution. *Lithos* 79, 1–24. doi:10.1016/j.lithos.2004.04.048

Maruyama, S., Isozaki, Y., Kimura, G., and Terabayashi, M. (1997). Paleogeographic maps of the Japanese slands: late tectonic synthesis from 750 Ma to the present. *Isl Arc.* 6, 121–142. doi:10.1111/j.1440-1738.1997.tb00043.x

Meschede, M. (1986). A methods of discriminating between different types of mid-ocean ridge basalts and continental tholeiites with the Nb−Zr−Y diagram. *Chem. Geol.* 83, 207–218. doi:10.1016/0009-2541(86)90004-5

Metcalfe, I. (2013). Gondwana dispersion and sian accretion: ectonic and palaeogeographic evolution of eastern ethys. *J. Asian Earth Sci.* 66, 1–33. doi:10.1016/j.jseaes.2012.12.020

Metcalfe, I. (2006). Palaeozoic and esozoic tectonic evolution and palaeogeography of East sian crustal fragments: he Korean eninsula in context. *Gondwana Res* 9, 24–46. doi:10.1016/j.gr.2005.04.002

Metcalfe, I. (2017). Tectonic evolution of undaland. *Bull. Geol. Soc. Malays* 63, 27–60. doi:10.7186/bgsm63201702

Moyen, J.-F. (2009). High Sr/Y and La/Yb ratios: he meaning of the "adakitic signature. *Lithos* 112, 556–574. doi:10.1016/j.lithos.2009.04.001

Nakano, N., Osanai, Y., Owada, M., Binh, P., Hokada, T., and Kaiden, H. (2021). Evolution of the Indochina block from its formation to amalgamation with Asia: constraints from protoliths in the Kontum Massif, Vietnam. *Gondwana Res* 90, 47–62.

Nam, T. N., Sano, Y., Terada, K., Toriumi, M., Van Quynh, P., and Dung, L. T. (2001). First SHRIMP U–Pb zircon dating of granulites from the Kontum massif (Vietnam) and tectonothermal implications. *J. Asian Earth Sci.* 19, 77–84. doi:10.1016/S1367-9120(00)00015-8

Nguyen, H., and Flower, M. (1998). Petrogenesis of enozoic basalts from Vietnam: mplication for origins of a 'diffuse igneous province. *J. Petrol.* 39, 369–395. doi:10.1093/petroj/39.3.369

Nguyen, T. T. B., Satir, M., Siebel, W., and Chen, F. (2004a). Granitoids in the Dalat zone, southern Vietnam: ge constraints on magmatism and regional geological implications. *Int. J. Earth Sci.* 93, 329–340. doi:10.1007/s00531-004-0387-6

Nguyen, T. T. B., Satir, M., Siebel, W., Vennemann, T., and Long, T. V. (2004b). Geochemical and isotopic constraints on the petrogenesis of granitoids from the Dalat zone, southern Vietnam. *J. Asian Earth Sci.* 23, 467–482. doi:10.1016/j.jseaes.2003.06.001

Nong, A. T. Q., Hauzenberger, C. A., Fallhofer, D., Skrzypek, E., and Dinh, S. Q. (2022). Geochemical and zircon U-Pb geochronological constraints on late Mesozoic Paleo-Pacific subduction-related volcanism in southern Vietnam. *Mineral. Petrol.* 116, 349–369. doi:10.1007/s00710-022-00785-z

Nong, A. T. Q., Hauzenberger, C. A., Gallhofer, D., and Dinh, S. Q. (2021). Geochemistry and zircon U-Pb geochronology of ate esozoic igneous rocks from SW ietnam-SE Cambodia: mplications for episodic magmatism in the context of the aleo-acific subduction. *Lithos* 390-391, 106101. doi:10.1016/j.lithos.2021.106101

Pearce, J. A., and Cann, J. R. (1973). Tectonic setting of basic volcanic rocks determined using trace element analyses. *Earth Planet. Sci. Lett.* 19, 290–300. doi:10.1016/0012-821X(73)90129-5

Pearce, J. A., Harris, N. B. W., and Tindle, A. G. (1984). Trace element discrimination diagrams for the tectonic interpretation of granitic rocks. *J. Petrol.* 25, 956–983. doi:10.1093/petrology/25.4.956

Plank, T., Kelley, K. A., Zimmer, M. M., Hauri, E. H., and Wallace, P. J. (2013). Why do mafic arc magmas contain ~4 wt% water on average? *Earth Planet. Sci. Lett.* 364, 168–179. doi:10.1016/j.epsl.2012.11.044

Rapp, R. P., Shimizu, N., Norman, M. D., and Applegate, G. S. (1999). Reaction between slab-derived melts and peridotite in the mantle wedge: xperimental constraints at 3.8 GPa. *Chem. Geol.* 160, 335–356. doi:10.1016/S0009-2541(99)00106-0

Rapp, R. P., and Watson, E. B. (1995). Dehydration melting of metabasalt at 8–32 kbar: mplications for continental growth and crust–mantle recycling. *J. Petrol.* 36, 891–931. doi:10.1038/s41467-022-34343-0

Roger, F., Maluski, H., Leyreloup, A., Lepvrier, C., and Thi, P. T. (2007). U–Pb dating of high temperature metamorphic episodes in the Kon Tum Massif (Vietnam). *J. Asian Earth Sci.* 30, 565–572. doi:10.1016/j.jseaes.2007.01.005

Rudnick, R. L., and Gao, S. (2014). Composition of the continental crust. *Treatise Geochem.* 4, 1–51.

Schellart, W. P., Chen, Z., Strak, V., Duarte, J. C., and Rosas, F. M. (2019). Pacific subduction control on Asian continental deformation including Tibetan extension and eastward extrusion tectonics. *Nat. Comm.* 10, 4480. doi:10.1038/s41467-019-12337-9

Scherer, E., Munker, C., and Mezger, K. (2001). Calibration of the utetium-afnium lock. *Science* 293, 683–687. doi:10.1016/0016-7037(95)00038-2

Shellnutt, J. G., Lan, C.-Y., Long, T. V., Usuki, T., Yang, H.-J., Mertzman, S. A., et al. (2013). Formation of retaceous ordilleran and post-orogenic granites and their microgranular enclaves from the Dalat zone, southern Vietnam: ectonic implications for the evolution of outheast Asia. *Lithos* 182-183, 229–241. doi:10.1016/j.lithos.2013.09.016

Shellnutt, J. G., Nguyen, D. T., and Lee, H.-Y. (2020b). Resolving the origin of the Seychelles microcontinent: nsight from zircon geochronology and Hf isotopes. *Precambrian Res.* 343, 105725. doi:10.1016/j.precamres.2020.105725

Shellnutt, J. G., Vaughan, M. W., Lee, H.-Y., and Iizuka, Y. (2020a). Late Jurassic leucogranites of Macau (SE China): record of crustal recycling during the arly anshanian rogeny. *Front. Earth Sci.* 8, 311. doi:10.3389/feart.2020.00311

Shi, M., Khin, Z., Liu, S., Xu, B., Meffre, S., Cong, F., et al. (2021). Geochronology and petrogenesis of arboniferous and riassic volcanic rocks in NW Laos: mplications for the tectonic evolution of the Loei Fold Belt. *J. Asian Earth Sci.* 208, 104661. doi:10.1016/j.jseaes.2020.104661

Sone, M., and Metcalfe, I. (2008). Parallel ethyan sutures in mainland southeast Asia: new insight for alaeo-ethys closure and implications for the ndosinian orogeny. *C. R. Geosci.* 340, 166–179. doi:10.1016/j.crte.2007.09.008

Straub, S. M., Gomez-Tuena, A., Stuart, F. M., Zellmer, G. F., Espinasa-Perena, R., Cai, Y., et al. (2011). Formation of hybrid arc andesites beneath thick continental crust. *Earth Planet. Sci. Lett.* 303, 337–347. doi:10.1016/j.epsl.2011.01.013

Straub, S. M., LaGatta, A. B., Martin-Del Pozzo, A. L., and Langmuir, C. H. (2008). Evidence from high-Ni olivines for a hybridized peridotite/pyroxenite source for orogenic andesites from the central Mexican volcanic belt. *Geochem. Geophys. Geosys.* 9, Q03007. doi:10.1029/2007GC001583

Suga, K., and Yeh, M.-W. (2020). Secular variation of arly retaceous granitoids in yushu, SW Japan: he role of mélange rocks as a possible magma source. *Front. Earth Sci.* 8, 95. doi:10.3389/feart.2020.00095

Sun, S. S., and McDonough, W. F. (1989). "Chemical and isotopic systematics of oceanic basalts: mplications for mantle composition and processes," in *Magmatism in the cean asins*. Editors A. D. Saunders and M. J. Norry (Bath, UK: Geological Society of London Special Publication), 313–435.

Taylor, B., and Hayes, D. E. (1983). "Origin and history of the South China Sea basin," in *The ectonic and eological volution of Southeast sian eas and slands: Part 2*. Editor D. Hayes (New York, USA: American Geophysical Union Geophysical Monograph), 23–56.

Tran, T. V., Faure, M., Nguyen, V. V., Bui, H. H., Fyhn, M., Nguyen, T. Q., et al. (2020). Neoproterozoic to arly riassic tectono-stratigraphic evolution of Indochina and adjacent areas: review with new data. *J. Asian Earth Sci.* 191, 104231. doi:10.1016/j.jseaes.2020.104231

Usuki, T., Lan, C.-Y., Wang, K.-L., and Chiu, H.-Y. (2013). Linking the Indochina block and Gondwana during the arly aleozoic: Evidence from U–Pb ages and Hf isotopes of detrital zircons. *Tectonophysics* 586, 145–159. doi:10.1016/j.tecto.2012.11.010

Waight, T., Fyhn, M. B. W., Thomsen, T. B., Tran, V. T., Nielsen, L. H., Abatzis, I., et al. (2021). Permian to retaceous granites and felsic volcanics from SW Vietnam and S Cambodia: mplications for tectonic development of Indochina. *J. Asian Earth Sci.* 219, 104902. doi:10.1016/j.seaes.2021.104902

Wang, K., Plank, T., Walker, J. D., and Smith, E. I. (2002). A mantle melting profile across the Basin and Range, SW USA. *J. Geophys. Res.* 107. doi:10.1029/2001JB000209

Wang, Y., Fan, W., Zhang, G., and Zhang, Y. (2013). Phanerozoic tectonics of the South China lock: ey observations and controversies. *Gondwana Res* 23, 1273–1305. doi:10.1016/j.gr.2012.02.019

Wang, Y., Qian, X., Cawood, P. A., Liu, H., Feng, Q., Zhao, G., et al. (2018). Closure of the ast aleotethyan cean and amalgamation of the eastern immerian and southeast Asia continental fragments. *Earth-Sci. Rev.* 186, 195–230. doi:10.1016/j.earscirev.2017.09.013

Whalen, J. B., Currie, K. L., and Chappell, B. W. (1987). A-type granites: eochemical characteristics, discrimination and petrogenesis. *Contrib. Mineral. Petrol.* 95, 407–419. doi:10.1007/BF00402202

Whalen, J. B., and Hildebrand, R. S. (2019). Trace element discrimination of arc, slab failure, and A-type granitic rocks. *Lithos* 348-349, 105179. doi:10.1016/j.lithos.2019.105179

White, L. T., and Lister, G. S. (2012). The collision of India with Asia. *J. Geodyn.* 56-57, 7–17. doi:10.1016/j.jog.2011.06.006

Wiedenbeck, M., Allé, P., Corfu, F., Griffin, W. L., Meier, M., Oberli, F., et al. (1995). Three atural ircon tandards for U-Th-Pb, Lu-Hf, race element and REE nalyses. *Geostand. Newslett.* 19, 1–23. doi:10.1111/j.1751-908X.1995.tb00147.x

Wu, J., Lin, Y.-A., Flament, N., Wu, J. T.-J., and Liu, Y. (2022). Northwest Pacific-Izanagi plate tectonics since Cretaceous times from Pacific mantle structure. *Earth Planet. Sci. Lett.* 583, 117445. doi:10.1016/j.epsl.2022.117445

Xia, X., Sun, M., Geng, H., Sun, Y., Wang, Y., and Zhao, G. (2011). Quasi-simultaneous determination of U-Pb and Hf isotope compositions of zircon by excimer laser-ablation multiple-collector ICPMS. *J. Anal. At. Spect.* 26, 1868–1871. doi:10.1039/C1JA10116A

Yang, Y.-T. (2013). An unrecognized major collision of the khotomorsk lock with East Asia during the ate retaceous, constraints on the plate reorganization of the orthwest acific. *Earth-Sci. Rev.* 126, 96–115.

Zaw, K., Meffre, S., Lai, C.-K., Burrett, C., Santosh, M., Graham, I., et al. (2014). Tectonics and metallogeny of mainland Southeast Asia – a review. *Gondwana Res* 26, 5–30. doi:10.1016/j.gr.2013.10.010

Zhao, D., Toyokuni, G., and Kurata, K. (2021). Deep mantle structure and origin of enozoic intraplate volcanoes in Indochina, ainan and South China Sea. *Geophys. J. Int.* 225, 572–588. doi:10.1093/gji/ggaa605

Zheng, H., Sun, X., Wang, P., Chen, W., and Yue, J. (2019). Mesozoic tectonic evolution of the roto-South China Sea: perspective from radiolarian pa`leobiogeography. *J. Asian Earth. Sci.* 179, 35–55. doi:10.1016/j.jseaes.2019.04.009

Zhou, X. M., and Li, W. X. (2000). Origin of ate esozoic igneous rocks in southeastern China: mplications for lithosphere subduction and underplating of mafic magmas. *Tectonophysics* 326, 269–287. doi:10.1016/S0040-1951(00)00120-7

Zhou, Z., Sun, T., Shen, W., Shu, L., and Niu, Y. (2006). Petrogenesis of esozoic granitoids and volcanic rocks in outh China: response to tectonic evolution. *Episodes* 29, 26–33. doi:10.18814/epiiugs/2006/v29i1/004